$A=18$ Nuclear Reaction Matrix*

S. KAHANA, H. C. LEE,†‡ AND C. K. SCOTT‡§
Brookhaven National Laboratory, Upton, New York 11973
(Received 13 February 1969)

The Brueckner reaction matrix for the $A=18$ nuclei is obtained in an accurate fashion from a nonlocal separable potential of the Tabakin type, but possessing a much stronger repulsive core. This potential, as well as those of Tabakin and Yamaguchi, is used in comparative studies of the reaction matrix. Both harmonic-oscillator and plane-wave intermediate states are employed. The results are compared extensively to the work by other authors on the local Hamada-Johnston potential. In the plane-wave treatment, the effect of replacing the kinetic-energy operator by a form (suggested by Baranger) more compatible with the exclusion principle is estimated.

I. INTRODUCTION

MANY authors[1] have in recent years attempted to deduce from the free-space nucleon-nucleon potential the residual interaction to be used in shell-model calculations. Inevitably, the initial approach is to take the effective interaction between valence nucleons to be the Brueckner reaction matrix defined in a strict ladder approximation.[2] Of couse, one tacitly assumes the existence of a self-consistent average field in which the core and valence particles move. Other workers[3] are attempting to justify this basic tenet of the shell model by performing a Hatree-Fock-like calculation embodying the Brueckner reaction-matrix theory.

Brown[4] suggested at the outset that an appreciable component of the residual interaction would obtain from a polarization of the supposedly inert closed shells. Kuo and Brown[1] and Kuo[5] have demonstrated this point for a variety of nuclei. Despite the non-negligibility of core polarization, it is evidently important to examine in detail the structure of the ladder approximation. It is the purpose of the present work to do just this with the aid of a separable potential which permits an essentially exact solution for the nuclear reaction matrix. It will be possible in the course of our studies to use a broad range of separable potentials and thus to check easily the effect on the residual interaction of varying prominent features of these potentials. In addition, we may readily alter the average field. It is of particular importance to be able to treat the occupied or hole states in a different fashion than the unoccupied or particle states. In what follows we employ harmonic-oscillator functions for the holes, but either oscillator functions or plane waves for the particles.

In an earlier work,[6] the present authors expanded the nuclear reaction matrix in terms of a phenomenologically-determined free reaction matrix. With the techniques presented here we are able to follow this expansion in detail, and to comment on two other approximate approaches to the nuclear reaction matrix: the reference-spectrum procedure of Bethe *et al.*[7] and the so-called phase-shift method.[8]

We must point out that our efforts parallel in many ways those of Wong.[9] Also, McCarthy[10] has recently performed similar computations. The work of these authors is distinguished from ours principally by their use of a local potential such as that of Hamada and Johnston (HJ).[11] The combined McCarthy-Wong results provide us with a complete analysis of the HJ potential, since Wong employed a plane-wave description of unoccupied nucleon states, whereas McCarthy used oscillator functions for all nucleon states. Setting their results against those we obtain permits us to make a thorough comparison of the residual interaction derived from local and nonlocal separable potentials.

II. TWO-PARTICLE POTENTIAL

Separable nucleon-nucleon potentials were first used by Yamaguchi[12] to obtain low-energy fits to the

* Work supported, in part, by U.S. Atomic Energy Commission.
† Permanent address: AECL, Chalk River Project, Chalk River, Ontario, Canada.
‡ These authors are grateful to the National Research Council of Canada for continued financial assistance while they were graduate students at McGill University, Montreal, Canada.
§ Permanent address: Niels Bohr Institute, Copenhagen, Denmark.

[1] J. F. Dawson, I. Talmi, and J. D. Walecka, Ann. Phys. (N.Y.) **18**, 339 (1962); S. Kahana, Nucl. Phys. **31**, 315 (1962); A. Kallio and K. Kolltveit, *ibid.* **53**, 87 (1964); A. D. MacKellar and R. L. Becker, Phys. Letters **18**, 308 (1965); S. Kahana and E. Tomusiak, Nucl. Phys. **71**, 402 (1965); T. T. S. Kuo and G. E. Brown, Phys. Letters **18**, 54 (1965); Nucl. Phys. **85**, 40 (1966); H. S. Kohler and R. J. McCarthy, *ibid.* **86**, 611 (1966); C. W. Wong, *ibid.* **A91**, 399 (1967). For a critical discussion of many aspects of this subject and a more complete bibliography, one might refer to the lectures delivered by M. Baranger at the International School of Physics (Enrico Fermi), Varenna, 1967 (unpublished).
[2] K. Brueckner, Phys. Rev. **97**, 1353 (1955).
[3] C. W. Wong, Nucl. Phys. **A104**, 417 (1967); K. T. R. Davies, M. Baranger, R. M. Tarbutton, and T. T. S. Kuo, *ibid.* (to be published).
[4] Private communication.
[5] T. T. S. Kuo, Nucl. Phys. **A103**, 71 (1967).
[6] S. Kahana and E. Tomusiak (see Ref. 1); H. C. Lee, M.S. thesis, McGill University, 1967 (unpublished); C. K. Scott, M.S. thesis, McGill University, 1967 (unpublished).
[7] H. A. Bethe, B. H. Brandow, and A. G. Petschek, Phys. Rev. **129**, 225 (1963).
[8] A. Kallio, Phys. Letters **18**, 51 (1965).
[9] C. W. Wong, Nucl. Phys. **A91**, 399 (1967).
[10] Private communication. We are greatly indebted to R. J. McCarthy for making available to us some of his results before publication.
[11] T. Hamada and I. D. Johnston, Nucl. Phys. **34**, 382 (1962).
[12] Y. Yamaguchi, Phys. Rev. **95**, 1628 (1954); Y. Yamaguchi and Y. Yamaguchi, *ibid.* **95**, 1635 (1954).

scattering and bound-state data. Later Tabakin[13] introduced more complex and more complete potentials of this nature to fit both the low- and high-energy data. We will employ a potential only slightly altered from the Tabakin form, but of a somewhat different character.[14] One of the primary concerns of Tabakin was to deduce a potential which could be used perturbatively in many nucleon investigations. Our potential will possess a stronger repulsive core than that used by Tabakin. It is our intention to use the Tabakin and Yamaguchi potentials, as well as our own, in comparative studies of nuclear matrix elements.

A general form for the potential we use may be given in terms of its momentum-space matrix elements

$$(\mathbf{k}\mid V\mid \mathbf{k}')=\sum_{ill'jsm\tau} g_{ll'(j)}{}^{i}v_l{}^{i}(k)v_{l'}{}^{i}(k') \times[\mathcal{Y}_{ls}{}^{jm}(\hat{k}\sigma)]^{*}[\mathcal{Y}_{l's}{}^{jm}(\hat{k}'\sigma')]P_{\tau}. \quad (1)$$

In Eq. (1), the potential is expanded in terms of angular functions

$$\mathcal{Y}_{ls}{}^{jm}(\hat{k}\sigma)=[Y_m{}^{l}(\hat{k})\chi^{s}(\sigma)]_m{}^{j}, \quad (2)$$

in which the relative orbital angular momentum l and the two-particle spin s have been coupled to total angular momentum j. We have also explicitly indicated a sum over the isobaric spin projection operators P_τ. Summations include only those states permitted by the exclusion principle. As a particular example we may isolate the potential form factor in the ${}^1S_0$ state

$$(k\mid V({}^1S_0)\mid k')=\sum_i g_{00(0)}{}^{i}v^{i}(k)v'(k'). \quad (3)$$

The summation in (3) may extend over as many terms i as one desires. In practice, we (like Tabakin) will limit ourselves to two terms: one attractive, one repulsive. The potential in the triplet spin states permits coupling between s and d waves via the coefficients $g_{02}=g_{20}$, and, hence, implicitly includes a tensor force.

The specific choice of the analytic form for the potential form factors in (2) and (3) distinguishes our potential from that of Tabakin. For the attractive parts of the potential $i=1$, we both employ

$$v_0{}^{1}(k)=(k^2+a_1{}^2)^{-1}, \quad (4)$$

as did Yamaguchi. Tabakin introduced a peak into the repulsive term with the choice

$$v_0{}^{2}(k)=k^2[(k-c)^2+a_2{}^2]^{-1}[(k+c)^2+a_2{}^2]^{-1}, \quad (5)$$

whereas we simply have

$$v_0{}^{2}(k)=[k^2+(a_2)^2]^{-1}. \quad (6)$$

The form factors (4) and (6) are used for both the uncoupled ${}^1S_0$ and the coupled ${}^3S_1$ states. For the ${}^3D_1$-wave form factor we have

$$v_2{}^{1,2}(k)=k^2[k^2+(a_2{}^{1,2})^2]^{-2}. \quad (7)$$

However, in other nonzero orbital angular momentum states, we take

$$v_l{}^{1}(k)=k^l[k^2+(a_l)^2]^{-(1+l/2)}, \quad (8)$$

$$v_l{}^{2}(k)=k^{(l+2}\infty[k^2+(a_l)^2]^{-(2+l/2)} \quad (9)$$

to simplify later integrations over these functions.

As we shall see, the fits to the two-body data obtained with (6) contain, in the s waves, a strong repulsive core. The latter rules out the later use of perturbation theory in the many-body problem.

A fit to the two-body data can be obtained by computing the free reaction matrix $K(\epsilon)$, which satisfies the scattering equation

$$K(\epsilon)=v+v[P/(\epsilon-t)]K(\epsilon), \quad (10)$$

where t is the relative kinetic-energy operator for a nucleon pair, P the principal-value operator, and ϵ an energylike parameter. On-the-energy-shell matrix elements of the free reaction matrix are directly related to the scattering phase shifts.

For the ${}^1S_0$ state one has, for example,

$$\tfrac{1}{2}\pi(k\mid K(\epsilon)\mid k')=-(\hbar^2/m)(1/k)\tan\delta_0(k), \quad \epsilon=\hbar^2k^2/m=\hbar^2k'^2/m. \quad (11)$$

In the coupled ${}^3S_1$ and ${}^3D_1$ states, the corresponding relationship is

$$i\tfrac{1}{2}\pi k(m/\hbar^2)K(\hbar^2k^2/m)=(1-S)(1+S)^{-1}, \quad (12)$$

where the S matrix may be described in terms of the Breit parametrization[15]

$$S=\begin{pmatrix}(1-\rho^2)^{1/2}\exp(2i\theta_{J-1}) & i\rho\exp[i(\theta_{J-1}+\theta_{J+1})]\\ i\rho\exp[i(\theta_{J-1}+\theta_{J+1})] & (1-\rho^2)^{1/2}\exp(2i\theta_{J+1})\end{pmatrix}. \quad (13)$$

Higher-orbital-angular-momentum states are treated in a similar fashion.

It is a straightforward task to insert the separable potential of Eq. (1) into (10) and obtain for the free reaction matrix in an uncoupled orbital state, a solution in the form

$$(k'\mid K_l(\epsilon)\mid k')=\sum_{i,i'} v_l{}^{i}(k)v_l{}^{i'}(k')\lambda_l{}^{ii'}(\epsilon). \quad (14)$$

The 2×2 matrix λ_l satisfies the equation

$$\lambda=(1-g\pi)^{-1}g, \quad (15)$$

[13] F. Tabakin, Ann. Phys. (N.Y.) **30**, 51 (1964).

[14] A similar potential fit has been obtained by T. R. Mongan [University of California Report, 1968 (unpublished)]. Mongan, however, uses the Arndt-McGregor (Livermore) data and, consequently, his potential differs slightly from ours.

[15] G. Breit, M. H. Hull, Jr., K. E. Lassila, and K. D. Pyatt, Jr., Phys. Rev. **120**, 2227 (1960).

TABLE I. Parameters of the separable potential. The values obtained in the s waves for the scattering length a_0 and effective range r_0 are given in the last two columns of this table. We have permitted a tensor coupling only in the $^3S_1$-$^3D_1$ waves. The $^3S_1$-$^3D_1$ potential labelled (a) predicts as a D-state probability for the deuteron $P_D=0.32\%$, whereas the potential labelled (b) results in $P_D=2.8\%$. An uncoupled fit to the $^3S_1$ wave is also presented with both a finite and an infinite strength g_2.

	a_1(F^{-1})	g_1/a_1 (MeV)	a_2(F^{-1})	g_2/a_2 (MeV)	a_0(F)	r_0(F)
			(a)			
$^3S_1$	1.593	-2.894×10^2	6.226	6.874×10^3	5.44	1.81
$^3S_1$-$^3D_1$		−78.05		1.527×10^4		
$^3D_1$	1.500	5.445×10^2	6.002	4.860×10^4		
			(b)			
$^3S_1$	1.4	-1.25×10^2	5	0.2×10^{10}	5.42	1.73
$^3S_1$-$^3D_1$		-1.78×10^2		0.63×10^9		
$^3D_1$	1.3	2.73×10^2	5	0.2×10^9		
$^1P_1$	1.90	4.401×10^2	1.90	4.577×10^5		
$^3D_2$	1.29	-2.052×10^2				
$^3D_3$	2.37	-2.562×10^2				
$^1S_0$	1.507	-1.912×10^2	7.29	7.775×10^3	−16.54	2.52
	1.505	-1.957×10^2	10.67	∞	−16.53	2.52
$^3P_0$	1.53	-2.069×10^2	1.53	8.856×10^2		
$^3P_1$	1.37	1.136×10^2	1.37	3.106×10^2		
$^3P_2$	1.57	−73.82	1.57	-1.727×10^2		
$^1D_2$	1.59	-1.214×10^2				
$^3S_1$	1.774	-4.947×10^2	8.526	9.491×10^6	5.39	1.77
(uncoupled)	1.706	-4.091×10^2	9.544	∞	5.39	1.78

where

$$g=\begin{pmatrix} g_l^1 & 0 \\ 0 & g_l^2 \end{pmatrix}; \tag{16}$$

while

$$\pi=\begin{pmatrix} \pi_l^{11} & \pi_l^{12} \\ \pi_l^{21} & \pi_l^{22} \end{pmatrix}, \tag{17}$$

with

$$\pi_l^{ii'}(\epsilon)=P\int_0^\infty q^2dq\, v_l^i(q)v_l^{i'}(q)[\epsilon-(\hbar^2/m)q^2]^{-1}. \tag{18}$$

We have permitted a tensor coupling in only the $^3S_1$ and $^3D_1$ states. For these states, Eq. (1) reduces to a form identical to (15), but now

$$g=\begin{pmatrix} g_{00} & g_{02} \\ g_{20} & g_{22} \end{pmatrix}, \tag{19a}$$

where

$$g_{ll'}=\begin{pmatrix} g_{ll'}^1 & 0 \\ 0 & g_{ll'}^2 \end{pmatrix}; \qquad l,l'=0,2 \tag{19b}$$

while

$$\pi=\begin{pmatrix} \pi_0 & 0 \\ 0 & \pi_2 \end{pmatrix} \tag{20a}$$

with

$$\pi_l=\begin{pmatrix} \pi_l^{11} & \pi_l^{12} \\ \pi_l^{21} & \pi_l^{22} \end{pmatrix}. \tag{20b}$$

The explicit forms for the $\pi_l^{ii'}$, resulting from Eqs. (4)–(9) and Eq. (18), are listed in the Appendix.

Since the solution presented in Eqs. (14) and (15) for $K(\epsilon)$ is a prototype of corresponding solutions obtained later for the Brueckner reaction matrix, we will present the explicit forms for $\lambda^{ii'}(\epsilon)$.

In the simplest case of the $^1S_0$ state,

$$\begin{aligned} \lambda^{11}&=(1-g^2\pi_0^{22})g^1[\Delta(\epsilon)]^{-1}, \\ \lambda^{12}&=\lambda^{21}=g^2g^1\pi_0^{12}[\Delta(\epsilon)]^{-1}, \\ \lambda^{22}&=(1-g^1\pi_{00}^{11})g^2[\Delta(\epsilon)]^{-1}, \end{aligned} \tag{21}$$

where

$$\Delta(\epsilon)=(1-g^1\pi_0^{11})(1-g^2\pi_0^{22})-g^1g^2(\pi_0^{12})^2.$$

One point which becomes evident from Eq. (21) is the finiteness of the free reaction matrix in the limit of an repulsive core, i.e., $g^2\to\infty$. One obtains, for example,

$$\lambda^{11}=g^1[\pi_0{}^{22}(1-g^1\pi_0{}^{11})+g^1(\pi_0{}^{11})^2]^{-1}\pi_0{}^{22}. \quad (22)$$

The nuclear reaction matrix deduced in Sec. III is also finite in this limit.

As one might expect from Eq. (10), the limit $\epsilon\to\infty$ for finite values of g^1 and g^2 leads to $\lambda^{ii'}\to\delta^{ii'}$, and hence to $K(\epsilon)\to v$. If, however, we first set $g_2=\infty$, then proceed to the limit $\epsilon\to\infty$, one obtains $\lambda^{ij}\sim\epsilon$, and the potential is not recovered for large ϵ. The behavior of $K(\epsilon)$ in the limit of large ϵ is of importance in our later discussion of the reference spectrum.

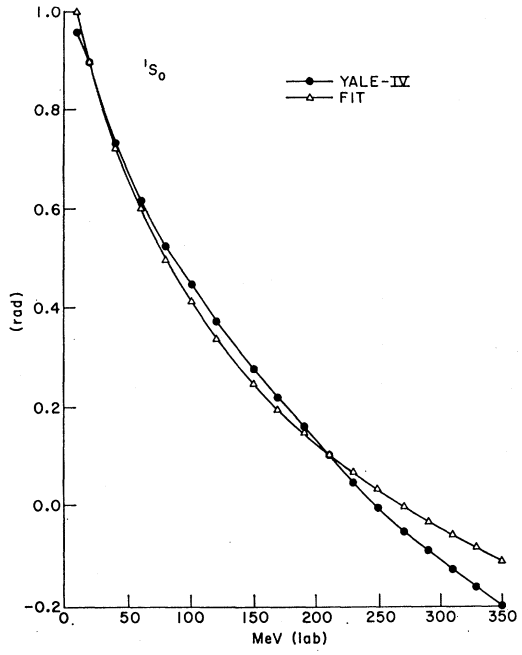

FIG. 1. Comparison of the Y-IV (Ref. 14) $^1S_0$ phase shift with the $^1S_0$ phase shift obtained from the finite core potential described in Table I. The quoted errors for the Y-IV data are too small to be indicated. The fit is made to proton-proton scattering data.

Our primary purpose in introducing $K(\epsilon)$ at this stage was to determine the potential parameters g^i and a^i. This can be accomplished by performing a least-squares fit of Eqs. (11) and (12) to the scattering data. We have chosen to use as a representation of the data, the phase shifts Y–IV of Breit *et al.*[16]

Our results are displayed in Table I, where the potential strength and range parameters are listed, and in Figs. 1–9, where graphs of the fits obtained with these parameters are shown. For comparison we have also presented in Table II some of the same parameters obtained by Yamaguchi and Tabakin. The original

[16] R. Seamon, K. A. Friedman, G. Breit, R. D. Haracz, J. M. Holt, and A. Prakash, Phys. Rev. 165, 1579 (1968).

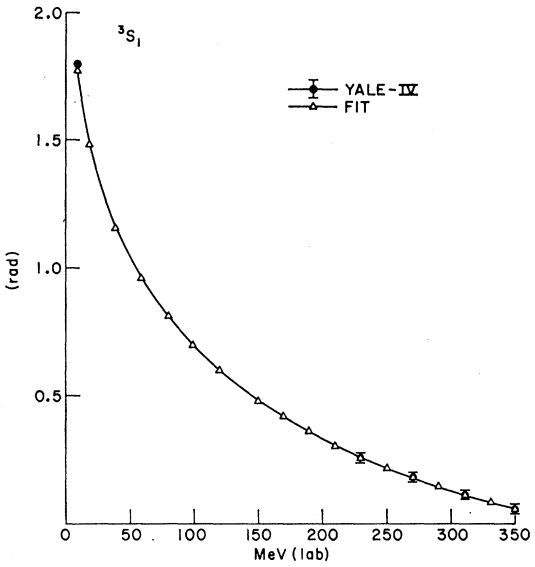

FIG. 2. Comparison of Y-IV (Ref. 14) phase fit $^3\theta_0{}^1$ with that obtained from our coupled $^3S_1$-$^3D_1$(a) potential. The two curves are indistinguishable. The Y-IV statistical errors are indicated by flags.

Tabakin fit[13] was to the YLAM and YLAN3M phase shifts.

When judged from the displayed graphs, the quality of our fit is relatively good. A possible exception is the fit to the $^3S_1$-$^3D_1$ coupling parameter ρ. What one cannot judge from the plotted curves is the accuracy of the fit

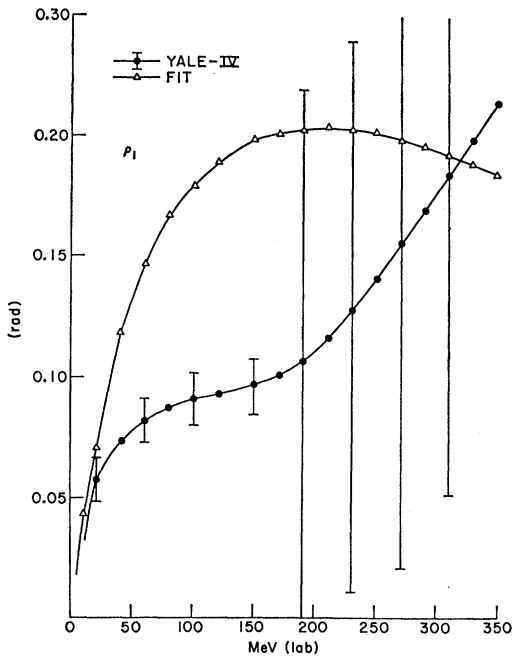

FIG. 3. Comparison of the Y-IV (Ref. 14) coupling parameter $\rho(^3S_1$-$^3D_1)$ with that obtained from our coupled $^3S_1$-$^3D_1$ (a) potential. The Y-IV (Ref. 14) errors are again indicated by flags. We have difficulties in fitting this parameter similar to those experienced by Tabakin.

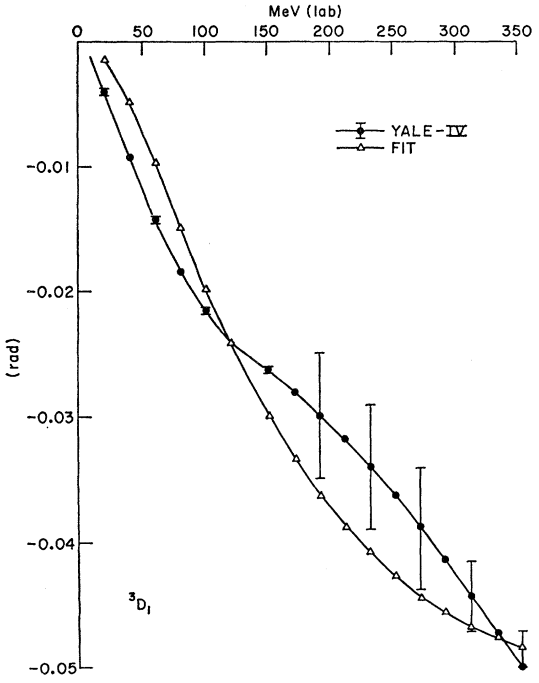

FIG. 4. Comparison of the Y-IV (Ref. 14) phase shift $^3\theta_2{}^1$ with that obtained from our coupled $^3S_1$-$^3D_1$ (a) potential.

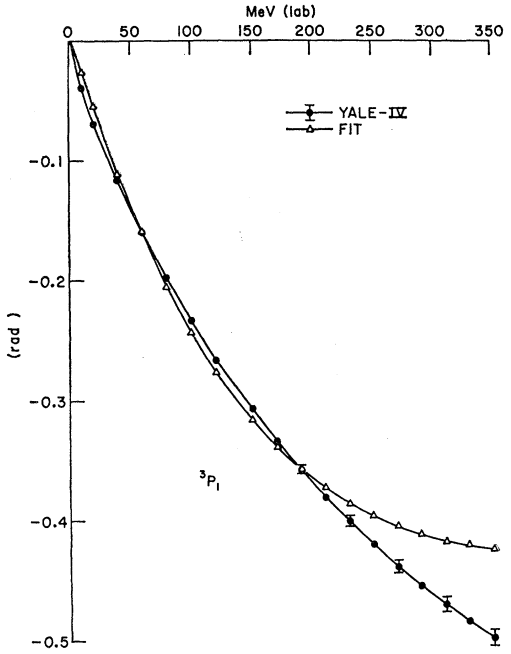

FIG. 6. Comparison of the Y-IV (Ref. 14) phase shift $^3P_1$ with that obtained from the $^3P_1$ potential parametrized in Table I.

at low energies. In all of our fits the scattering lengths and effective ranges are accurately predicted, but the deuteron is not considered directly. Indeed we find the coupled $^3S_1$-$^3D_1$ potential parameters (a) listed in Table I, predict a D-state probability for the deuteron of only 0.3%. To increase this parameter P_D to a more reasonable value, say between 3% and 4%, we made slight modifications in our potential. One minor change was the use of the repulsive form factor (7) for the ^3S wave, as well as for the ^3D wave. A more major alteration was to determine the strength of the $^3S_1$-$^3D_1$ coupling strengths $g_{02}{}^{1,2}$ from the relations

$$(g_{02}{}^1)^2 = -g_0{}^1 g_2{}^1$$
$$\text{and} \qquad (g_{02}{}^2)^2 = g_0{}^2 g_2{}^2. \qquad (23)$$

Aside from the negative sign associated with $(g_{02}{}^1)^2$, these latter relations are those proposed by Yamaguchi

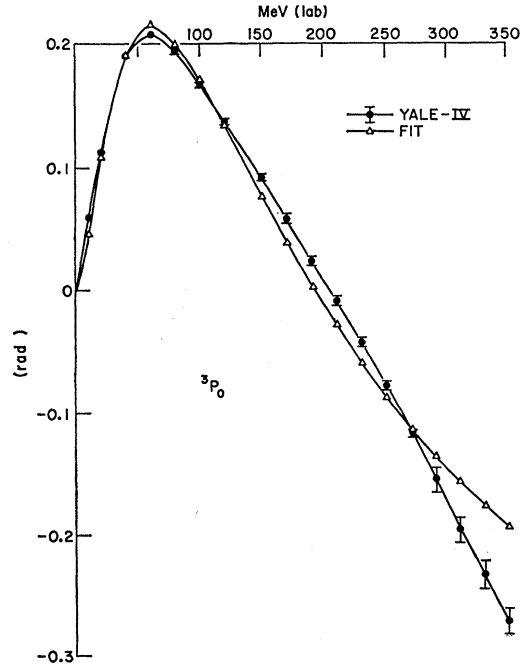

FIG. 5. Comparison of the Y-IV (Ref. 14) phase shift $^3P_0$ with that obtained from the $^3P_0$ potential parametrized in Table I.

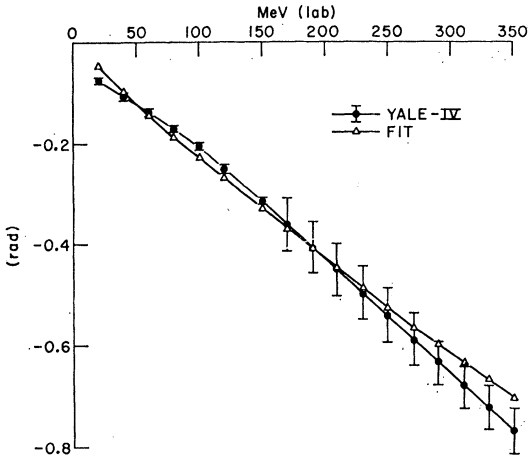

FIG. 7. Comparison of the Y-IV (Ref. 14) phase shift $^1P_1$ with that obtained from the $^1P_1$ potential in Table I.

and Yamaguchi[12] and used by these authors and by Tabakin. It is interesting that the potential parameters $^3S_1$ (a) which yield too small a value of P_D predict a coupling parameter ρ which is, if anything, too large for laboratory scattering energies above 20 MeV. The strength of the tensorlike constant g_{02} in this latter fit (a) falls well below the value necessary for satisfying Eq. (23). When we impose Eq. (23), thus increasing the relative strength of our tensor force and presumably also raising the value of P_D, we find it even more difficult to fit the parameter ρ at high energies. This failing, apparently characteristic of the nonlocal potentials we are employing, could perhaps be eliminated by adding a third separable term to our coupled $^3S_1$-$^3D_1$ potential.

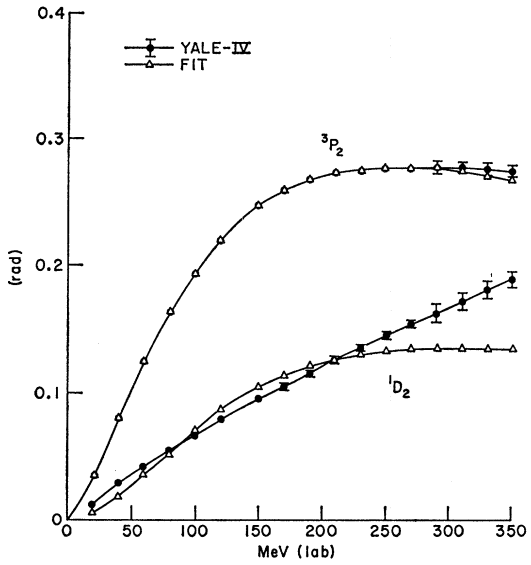

FIG. 8. Comparison of the Y-IV (Ref. 14) phase shifts $^3P_2$ and $^1D_2$ with those obtained from the corresponding potentials in Table I.

The choice of sign made for $(g_{02}{}^1)^2$ in Eq. (23) is motivated by the desire to use two repulsive, separable terms in the $^3D_1$ potential. In fact, the slightly repulsive phase shifts observed experimentally in this channel are one possible argument for a strong $^3S_1$-$^3D_1$ tensor force. A purely central force must certainly be strong and attractive to correctly predict the $^3S_1$ bound-state and scattering data. A tensor force which is capable of overwhelming the central force in the $^3D_1$ state, leaving a residual repulsive force, must also be strong.

The coupled $^3S_1$-$^3D_1$ potential parameters, labelled (b) in Table I, predict a D-state probability of 2.8%, but lead to phase shifts which are not quite as good a fit to the experimental data as those deduced from potential (a). It is unlikely, however, that a further refining of this potential will appreciably alter the nuclear matrix elements that will eventually be calculated. We were able by slight variations in the potential strengths and in the range $a_2{}^2$ to reduce P_D to 2.0%, retaining,

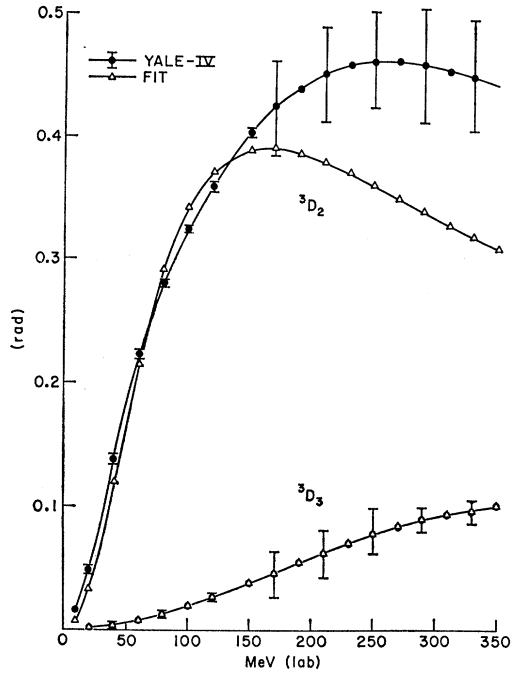

FIG. 9. Comparison of the Y-IV (Ref. 14) phase shifts $^3D_2$ and $^3D_3$ with those obtained from the corresponding potentials in Table I.

however, the relations of Eq. (23). In the present work, we present the results obtained with the potential (b), since its tensor component probably represents an extreme upper limit in strength. In any case we found only minor differences in nuclear calculations between the potentials with $2\%<P_D<3\%$. Once the relation (23) is imposed it would appear one obtains a stronger tensor component.

It is, of course, difficult to directly compare separable nonlocal potentials with more conventional local potentials. We felt the introduction of a strong repulsive core would render our particular version of the nonlocal potential closer in nature to the HJ potential than was the Tabakin version. One distinctive feature of the

TABLE II. Parameters for the S-wave Yamaguchi and Tabakin potentials. The notation for the Tabakin potential is that of Eqs. (4) and (5). The strengths g in Table II for the Tabakin potential are related to those quoted by Tabakin (Ref. 3), g_T, by $g=(2/\pi)g_T$.

	a_1 (F^{-1})	g_1/a_1 (MeV)	a_2 (F^{-1})	g_2/a_2 (MeV)	c (F^{-1})
		Yamaguchi			
$^1S_0$	1.449	−83.92			
$^3S_1$	1.274	−80.33			
		Tabakin			
$^1S_0$	1.207	−73.78	1.104	149.98	1.441
$^3S_1$	1.73	−104.85	1.01	6.56	1.695

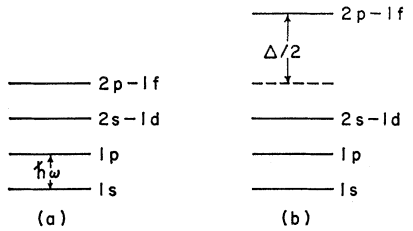

FIG. 10. The single-particle oscillator spectrum used in the ladder approximation (a) without an energy gap (b) with a gap $\Delta/2$. The occupied states are $1s$ and $1p$, valence states are $2s-1d$ and unoccupied or particle states $\geq 2p-1f$. The oscillator energy parameter was $\hbar\omega=13.4$ MeV for the $A=18$ nuclei.

separable potentials does arise in the course of actually fitting them to the data. Insofar as one can refer to a range for these potentials, this range seems definitely shorter than that of the local potentials. The latter are, in fact, generally matched at large nucleon separations to the one-pion-exchange potential (OPEP). Most notably, the HJ potential possesses a strong tensor force with the OPEP range of 1.4 F, whereas our coupled $^3S_1$-$^3D_1$ potentials contain a tensor force with a range of the order of 0.6 F.

III. NUCLEAR REACTION MATRIX

A. Direct Evaluation

The residual interaction in this paper is simply the Brueckner reaction matrix obtained from the ladder approximation. For the case of two valence nucleons outside closed shells, the equation satisfied by this reaction matrix is

$$K_N(E)=v+v[Q/(E-H_0)]K_N(E), \qquad (24)$$

where $H_0=H_0(1)+H_0(2)$ is the two-particle shell-model Hamiltonian. We will consider in this work a diagonalization of the residual interaction within the $2s$-$1d$ shell. Hence, the operator Q eliminates not only the occupied $1s$ and $1p$ shell-model states, but also states in which both valence particles are in the $2s$-$1d$ shell. We are then considering matrix elements of $K_N(E)$ which are appropriate to the mass-18 nuclei O^{18} and F^{18}. It is conceivable that for such nuclei one might desire to enlarge the zero-order space to include the $1f$-$2p$ shell, in which case the operator Q would be adjusted accordingly.

Perhaps the most crucial issue in solving Eq. (24) is the selection of the single-particle spectrum. Normally, one imagines H_0, which represents the interaction, between valence particles and the closed shells, to be obtained in some self-consistent fashion. In practice, one assigns a definite parametrized form to H_0 and determines these parameters from existing data on the single-valence-particle nuclei O^{17} and F^{17}. Naively one might expect the spectrum of $H_0(1)$ to appear as in Fig. 10(a). This spectrum will result if one takes in Eq. (24), $E=E_{sd}$, the energy of the pair of valence nucleons in the sd shell. If one selects an oscillator form for H_0, then $E_{sd}=2\times\frac{7}{2}\hbar\omega$, and the more or less constant spacing between major shells in Fig. 10(a) is $\hbar\omega$. For the $1s$-$2d$ shell we have chosen the value $\hbar\omega=13.4$ MeV.

One must recall that Eq. (24) has arisen from a many-body calculation and H_0 is very much a consequence of nature of the approximations made in this calculation. The energies of unoccupied or particle states, i.e., the $2p$-$1f$ and higher shells, are not necessarily those to be expected if a nucleon occupied these levels. To enhance the convergence of the Goldstone series for the total energy in nuclear matter, it has been suggested that the particle potential energies be omitted.[17] These energies are, in fact, better discussed in the context of three-body correlations.[18] When the latter are considered in totality, it is felt that the particle potential energies may be redundant. This is a controversial point the resolution of which is still, perhaps, in doubt for the treatment of nuclear matter, and certainly unresolved for finite nuclear considerations.

In view of the last paragraph, we are led to examine the single-particle spectrum [Fig. 10(b)] which result from the choice $E=E_{sd}-\Delta$, where Δ is some preassigned energy gap between hole and particle states. To facilitate a later comparison with a calculation involving plane-wave particle states, it would be well to set the unperturbed position of the degenerate $2s$-$1d$ shell at the true zero of energy for a nucleon in the mass-17 nuclei, i.e., where this nucleon becomes unbound. We have, in fact, made the selection

$$E=E'+E_{sd}-\Delta, \qquad (25)$$

where E' is the binding energy of the pair of valence nucleons in the $A=18$ nucleus relative to the energy of the O^{16} core. The variation of E' over the configurations of the s-d shell is reflected in a state dependence of the residual interaction $K_N(E)$. We have made the state-independent choice $E'=-13$ MeV, corresponding more or less to the ground-state binding energy in O^{18} or F^{18}. The results of varying E' by ± 5 MeV led us to conclude that this particular state dependence is small, at least for the forces we consider.

As we have indicated, an alternative treatment of the particle states is to describe them with plane waves orthogonalized to the localized oscillator functions retained for occupied states. This point of view, which is also that of Wong,[9] will be treated in detail in Sec. V of this work.

In the first instance, we will discuss Eq. (24) with a pure oscillator form for H_0. The matrix elements of $K_N(E)$, which are to be used in a residual-interaction diagonalization in the s-d shell, may then be presented to exhibit explicitly their dependence on two-body

[17] G. E. Brown, G. T. Schappert, and C. W. Wong, Nucl. Phys. **56**, 191 (1964); P. C. Bhargava and D. W. L. Sprung, Ann. Phys. (N.Y.) **42**, 222 (1967).

[18] R. Rajaraman, Phys. Rev. **129**, 265 (1963); H. A. Bethe, *ibid.* **138B**, 804 (1965).

relative and c.m. coordinates. If the single-particle oscillator states are labelled by the usual quantum numbers $\{\sigma\}=j_\sigma m_\sigma l_\sigma \tau_\sigma$, to calculate spectra would require a knowledge of the matrix elements,

$$\langle(\sigma_1\sigma_2)^{JT}|\bar{K}_N(E)|(\sigma_1'\sigma_2')^{JT}\rangle. \tag{26}$$

However, we may concentrate on

$$\langle[(nls)^jNL]^{JT}|K_N(E)|[(n'l's')^{j'}N'L']^{JT}\rangle, \tag{27}$$

where nl are the relative, radial and orbital quantum numbers for oscillator wave functions, and NL the corresponding c.m. quantities. In the future, we will generally suppress the labels of total angular momentum and isobaric spin JT, and other labels whose presence can be inferred. In (27) the two-particle spin s has been coupled to the relative orbital angular momentum l in a fashion obviously convenient for considering matrix elements of the free two-body potential.

The explicit transformation connecting (26) and (27) is

$$\begin{aligned}\langle(\sigma_1\sigma_2)^{JT}|K_N(E)|(\sigma_1'\sigma_2')^{JT}\rangle&=\sum((l_1\tfrac{1}{2})^{j_1}(l_2\tfrac{1}{2})^{j_2}|(l_1l_2)^{\Lambda}(\tfrac{1}{2}\tfrac{1}{2})^s)\\&\times((l_1'\tfrac{1}{2})^{j_1'}(l_2'\tfrac{1}{2})^{j_2'}|(l_1'l_2')^{\Lambda'}(\tfrac{1}{2}\tfrac{1}{2})^s)_J\\&\times(n_1l_1n_2l_2,\Lambda\,|\,nlNL,\Lambda)(n_1'l_1'n_2'l_2',\Lambda'\,|\,n'l'N'L',\Lambda')\\&\times U(LlJs;\Lambda j)U(L'l'Js,\Lambda'j')\\&\times([(nls)^jNL]^{JT}|K_N(E)|[(n'l's)^{j'}N'L']^{JT})\\&\times 2(1+\delta_{\sigma_1\sigma_2})^{-1/2}(1+\delta_{\sigma_1'\sigma_2'})^{-1/2},\end{aligned} \tag{28}$$

where $((l_1\frac{1}{2})^{j_1}(l_2\frac{1}{2})^{j_2}|(l_1l_2)^{\Lambda'}(\frac{1}{2}\frac{1}{2})^s)$ is the standard ls-jj transformation coefficient,[19] $(n_1l_1n_2,\Lambda\,|\,nlNL,\Lambda)$ the Brody-Moshinsky transformation coefficient,[20] and $U(LlJs;\Lambda j)$ the Racah coefficient.[21] Antisymmetrization and normalization of the two-particle states in (28) requires one to include the last factor in (28).

The major difficulty in solving Eq. (24) is, of course, the coupling between c.m. and relative coordinates brought about by the operator Q. One can again apply the transformation of Eq. (28) to the single-particle intermediate states $|\sigma_1\sigma_2\rangle$ of Eq. (24). The result is

$$\begin{aligned}\langle(nls)^jNL|K_N(E)|(n'l's)^{j'}N'L'\rangle&=\langle(nls)^j|v|(n'l's)^j\rangle\delta_{NN'}\delta_{LL'}\delta_{jj'}\\&+\sum_{n''l'',n'''l''',N'''L''',\Lambda''\Lambda'''}\langle(nls)^j|v|(n''l''s)^j\rangle\\&U(L''l''Js;\Lambda''j)U(L'''l'''Js;\Lambda'''j''')\\&\times(n''l''NL,\Lambda''\,|\,Q\,|\,n'''l'''N'''L''',\Lambda''')\\&\times[E-E(n''l''NL)]^{-1}\\&\times\langle(n'''l'''s)^{j'''}N'''L'''|K_N(E)|(n'l's)^{j'}N'L'\rangle,\end{aligned} \tag{29}$$

where

$$\begin{aligned}&(n''l''NL,\Lambda''\,|\,Q\,|\,n'''l'''N'''L''',\Lambda''')\\&\quad=\sum_{n_1l_1n_2l_2}{}'(n_1l_1n_2l_2,\Lambda''\,|\,n''l''NL,\Lambda'')\\&\qquad\times(n_1l_1n_2l_2,\Lambda'''\,|\,n'''l'''N'''L''',\Lambda'''),\end{aligned} \tag{30}$$

and

$$E(n''l'',NL)=E(n_1l_1n_2l_2)=\hbar\omega(2n''+l''+2N+L+3).$$

The primed summation in Eq. (30) proceeds over those states permitted by the exclusion principle as discussed before, but also is limited to those states possessing a fixed total number of oscillator quanta.

A major simplification in the very general Eq. (29) is obtained by use of the separable potential (1). One can employ an ansatz similar to Eq. (14) for the free reaction matrix, i.e.,

$$\begin{aligned}&\langle(nls)^jNL|K_N(E)|(n'l's)^{j'}N'L'\rangle\\&=\sum_{ii'=1}^{2}v_{js}{}^i(nl)v_{j's}{}^{i'}(n'l')\langle NL_i\,il|\lambda_N(E)|N'L',i'l'\rangle,\end{aligned} \tag{31}$$

where $v_{js}{}^i(nl)=\int R_{nl}(k)v_{js}{}^i(k)k^2dk$ and $R_{nl}(k)$ is the normalized Fourier transform of the oscillator relative wave function. This ansatz reduces Eq. (29) to

$$\lambda_N(E)=1+g\pi_N(E)\lambda_N(E). \tag{32}$$

In Eq. (32) the matrix indices are collectively labelled by $(\alpha)\equiv(NLil)$, while g and $\pi_N(E)$, respectively, have the matrix elements

$$g_{\alpha\alpha'}=\langle NL,il\,|\,g\,|\,N'L'i'l'\rangle=\delta_{ii'}\delta_{NN'}\delta_{LL'}g_{ll'}{}^i \tag{33}$$

and

$$\begin{aligned}&\langle NL,il\,|\,\pi_N(E)|\,N'L',il'\rangle\\&=\sum_{nn'}v_{js}{}^i(nl)U(LlJs;\Lambda j)(nlNL,\Lambda\,|\,Q\,|\,n'l'N'L',\Lambda')\\&\times[E-E(nl,NL)]^{-1}U(L'l'Js;\Lambda'j')v_{j's}{}^{i'}(n'l').\end{aligned} \tag{34}$$

If the inclusion of the relative orbital c.m. in the index α were only motivated by the tensorlike coupling that exists in Eq. (29) between l and l'' (or l' and l''') for triplet spin, then the solution of Eq. (32) would be relatively straightforward. However, the nondiagonality of Q in l'' and l''', operative in the general situation for which forces exist in all partial waves, is a formidable computational problem to surmount. If, while treating the relative states ${}^1S_0$ or $({}^3S_1,{}^3D_1)$, we discount the forces in other partial waves, then coupling to other partial waves through Q is eliminated. Alternatively, we can simply dismiss the off-diagonality in orbital angular momentum, thus, essentially, employing the angle-averaging approach to nuclear matter. We will use the angle-averaged Q for calculations in the higher-orbital states.

To illustrate our procedure for the solution of Eq. (32) we refer to the simplest case of a singlet spin state.

[19] J. M. Kennedy and M. J. Cliff, AECL Report, Chalk River, Canada, 1955 (unpublished).

[20] J. A. Brody and M. Moshinsky, *Tables of Transformation Brackets* (Monográfias del Instituto de Fisica, Mexico, 1960).

[21] G. Racah, Phys. Rev. **62**, 438 (1942).

TABLE III. Some representative matrix elements of the Pauli operator Q for increasing values of the total oscillator quantum number $\nu=2n+l+2N+L=2n'+l'+2N'+L'$. For diagonal matrix elements the c.m. and relative quantum numbers are listed only once. Quantum numbers which are being repeated are simply omitted. In column (a) are listed the matrix elements obtained using Eq. (30) without approximation. Column (b) contains the same matrix elements angle-averaged according to Eq. (40). When the (a) and (b) values are clearly identical the (b) values are omitted. Despite the drastic averaging which occurs in some cases the diagonal $K_N(E)$ matrix elements are much the same whether one uses (a) or (b).

		Q values									
ν	Λ	n	l	N	L	n'	l'	N'	L'	(a)	(b)
6	0	3	0	0	0					0.781	
8		4								0.930	
10		5								0.978	
12		6								0.993	
14		7								0.998	
16		8								0.999	
6	4	1	0	0	4					0.531	
8		2								0.696	
10		3								0.816	
12		4								0.897	
14		5								0.946	
16		6								0.974	
18		7								0.988	
6	0	2	1	0	1					0.312	0.625
	1									0.875	
	2									0.538	
8	0	3	1	0	1					0.656	0.838
	1									0.968	
	2									0.797	
12	0	5	1	0	1					0.945	0.977
	1									0.998	
	2									0.971	
6	0	3	0	0	0	2	0	1	0	−0.248	0
						1		2		0.083	0
						0		3		0.156	0
8	0	4	0	0	0	3	0	1	0	−0.135	0
						2		2		−0.039	0
						1		3		+0.081	0
						1		4		+0.055	0
10	0	5	0	0	0	4	0	1	0	−0.059	0
						3		2		−0.047	0
						2		3		0.016	0
						1		4		0.041	0
14	0	7	0	0	0	6	0	1	0	−0.008	0
						5		2	0	−0.014	0

For this case,

$$\langle NLi \mid \pi_N(E) \mid N'L'i' \rangle = \sum_{n''} v^i(n''0)[E-E(n''0NL)]^{-1} \times (n''0NL, L \mid Q \mid n'''0N'L, L) v^{i'}(n'''0), \quad (35)$$

with

$$J=L=L',$$

while

$$2n''+2N=2n'''+2N'.$$

If at this point we were to assume that Q were completely diagonal in the c.m. quantum numbers, the matrix index α would collapse to the single label i. Equation (32) would then be a 2×2 matrix equation identical in form to Eq. (15), and its solution would be given by Eqs. (21). It may be noted that our procedures most closely parallel the so-called "global" approximation of Wong, and that the completely diagonal assumption for Q is Wong's approximation $GA(0)$.

It is evident that the any nondiagonality in $(nlNL, \Lambda \mid Q \mid n'l'N'L, \Lambda')$ must disappear as one considers increasingly larger values of $\nu=2n+l+2N+L=2n'+l'+2N'+L'$. In this limit the sum in Eq. (30) becomes unrestricted. In practice, for $\nu>14$ one can effectively take $Q=1$. Some representative matrix elements of Q calculated using (30) are presented in Table III. With Wong, we, in fact, find that $GA(0)$ is generally an excellent approximation for calculating matrix elements of K_N, which are themselves diagonal in the c.m. coordinates.

A second computational point to be considered is the specific evaluation of the part of the summation in Eq. (35) arising from large values of n''. One has (approximately) for this summation

$$\sum_{n''>n_0} v^i(n''0)[E-E(NL)-(2n''+\tfrac{3}{2})\hbar\omega]^{-1}v^{i'}(n''0). \quad (36)$$

For short-ranged nuclear forces this contribution to $\pi_N(E)$ is considerable. Indeed, for a zero-range force the summation diverges. One may convert this summation into an easily evaluated integration by employing the following approximation:

$$v^i(n0)\approx(\hbar/m\omega)\,k_n^{1/2}v^i(k_n), \quad (37)$$

where

$$\hbar^2k_n^2/m=(2n+\tfrac{3}{2})\hbar\omega.$$

This result is arrived at by noting that a relative oscillator wave function $R_{n0}(r)$ used in conjunction with a short-ranged potential function $v(r)$ is well approximated by[22]

$$R_{n0}(r)\approx[2(2)^{1/2}\Gamma(n+\tfrac{3}{2})/2\pi n!]^{1/2}j_0(k_nr).$$

Equation (37) then follows in the limit of large n. We

[22] A. Kallio, Phys. Letters **18**, 51 (1965).

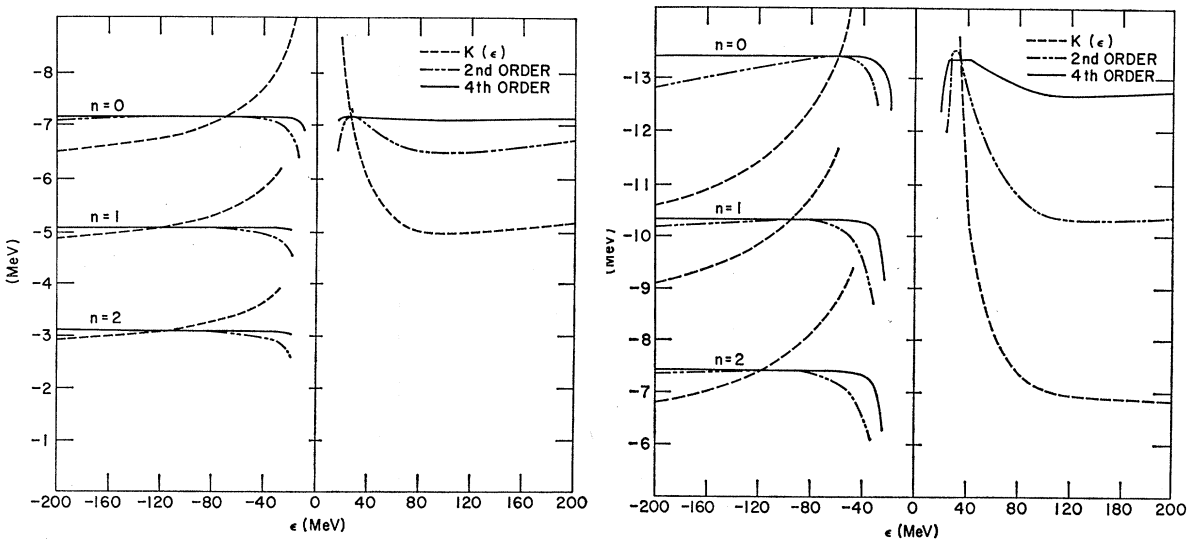

FIG. 11. (a) The expansion of $^1S_0$ matrix elements of $K(E)$ deduced from a gapless oscillator spectrum and the finite-core potential in Table I as a series in the free reaction matrix $K(\epsilon)$. The $n=1$, 2 matrix elements are not shown for $\epsilon>0$, but behave in a manner similar to the $n=0$ matrix element. (b) The expansion of $^3S_1$ matrix elements of $K_N(E)$ deduced from a gapless oscillator spectrum and the potential $^3S_1$-$^3D_1$ (a) in Table I as a series in the free reaction matrix $K(\epsilon)$.

then have

$$\sum_{n''\geq n_0}^{\infty} v^i(n'0)[E-E(NL)-(2n''+\tfrac{3}{2})\hbar\omega]^{-1}v^{i'}(n''0)$$

$$\approx \int_{kn_0}^{\infty} k^2dk\, v^i(k)v^{i'}(k)[E-E(NL)-(\hbar^2k^2/m)]^{-1}. \quad (38)$$

The accuracy of the foregoing approximation was demonstrated by varying the choice of the point $n=n_0$ at which one converts the summation to an integration.

Once the matrix elements of $\pi_N(E)$ are computed they may be inserted into Eq. (32) to yield $\lambda_N(E)$, and ultimately $K_N(E)$.

B. Expansion of $K_N(E)$ as a Series in $K(\epsilon)$

Reference Spectrum

Before presenting the nuclear reaction matrix elements calculated according to the procedures just described, we wish to consider, in a parallel treatment, an evaluation of these same matrix elements from an expansion of $K_N(E)$ in terms of $K(\epsilon)$. This procedure was outlined in previous work by the present authors, and by Kahana and Tomusiak.[6] Equations (1) and (24) may be easily manipulated to yield

$$K_N(E)=K(\epsilon)+K(\epsilon)\left(\frac{Q}{E-H_0}-\frac{P}{\epsilon-t}\right)K_N(E)$$

$$=K(\epsilon)+K(\epsilon)\left(\frac{Q}{E-H_0}-\frac{P}{\epsilon-t}\right)K(\epsilon)+\cdots. \quad (39)$$

For negative values of the parameter ϵ the above expansion is equivalent to the reference-spectrum procedure of Bethe *et al.*[7] We have considered the expansion (39) up to fourth order in $K(\epsilon)$ for both positive and negative ϵ in a broad range, and for a vanishing gap, $\Delta=0$. The results are presented in Fig. 11(a) for the $^1S_0$ matrix elements deduced from a potential, with a finite core, and in Fig. 11(b) for the coupled $^3S_1$ matrix elements obtained from potential (a) of Table I. The corresponding curves obtained using infinite cores or an uncoupled $^3S_1$ wave are not sufficiently different to be plotted separately. The dependence of $K(\epsilon)$ on ϵ for the states $^1P_1$, $^3D_2$, $^3D_3$, in which the force is somewhat weaker, is shown in Fig. (12).

The convergence of the series in the free reaction matrix, indicated in Fig. 11(b) for the $^3S_1$ states, is much the same whether one employs the potential (a)

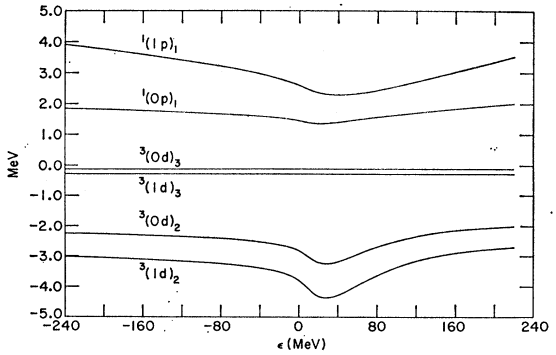

FIG. 12. Free reaction matrix elements for the states $^1P_1$, $^3D_3$, $^3D_2$ deduced from the potentials in Table I.

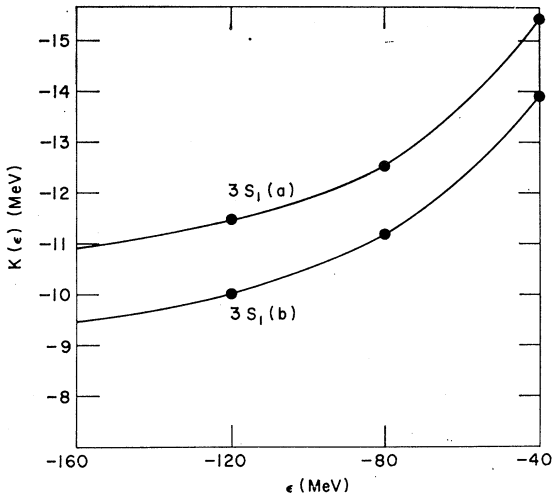

FIG. 13. Comparison between the $^3S_1$, $n=0$ reference-spectrum matrix elements deduced from our $^3S_1$-$^3D_1$ potentials (a) and (b).

of Table I with $P_D=0.3\%$, or the potential (b) with $P_D=2.8\%$. In Fig. 13, we have displayed the $n=0$, $^3S_1$ lowest-order reference-spectrum matrix elements of these two potentials. The introduction of a stronger tensor force at low energies seems to have reduced the magnitude of this matrix element, but not to have altered its rate of fall off with increasing (ϵ). The same may be said of the $n=1$ and $n=2$ matrix elements.

To further explore the dependence of the reference spectrum on the underlying potential we have, in Table IV, listed the reference-spectrum matrix elements extracted from our $^1S_0$, $^3S_1$ (a), and $^3S_1$ (b) potentials as well as from the local HJ potential.[9] One observes that the matrix elements $\langle n0; NL \mid K(\epsilon) \mid n0, NL\rangle$ arising from the HJ potential fall off more quickly for increasing negative values of $\epsilon=-\gamma^2\times(40\text{ MeV})$ or for increasing n. An examination of the explicit forms for the functions $\pi^{ii'}(\epsilon)$ listed in the Appendix indicates that these functions depend on the ranges a^i through the parameters $(a^i)^2\epsilon m/\hbar^2$. Thus, the energy scale of the free reaction matrix is determined by the range of the potential. As one allows $\epsilon\rightarrow-\infty$, one expects the repulsive parts of the potential to become increasingly more important. For a nonsingular potential Eq. (10) yields $K(\epsilon)\rightarrow v$, as $\epsilon\rightarrow-\infty$. The longer the range of the attractive part of the potential, the more quickly will the dominance of the shorter-range repulsive force be felt. The HJ s-state forces contain at least the OPEP long-ranged components. In the $^3S_1$ matrix elements, where the HJ long-ranged tensor force is of crucial importance, the drop with γ^2 or n is most evident. Of course, this argument must be tempered by the restrictions placed on the free reaction matrix at positive energies. Coefficients of the scaling parameters $(a^i)^2\epsilon m/\hbar^2$ are not independent of the ranges a^i, if one is to fit the scattering data. It may also be true that the HJ repulsive core is in some senses harder than ours, and that the local nature of the HJ potential enhances the above range effect.

One also sees from Table IV, that the insertion of a stronger tensor force into the separable potential has produced a reduction in amplitude of the $n=0$ $^3S_1$ reference-spectrum matrix element. The remaining differences at fixed ϵ between this matrix element and the corresponding matrix elements obtained from the HJ potential must be ascribed to some other source.

Finally, it is easy to demonstrate that the dependence of reference matrix elements on n may be linked to the range of the attractive part of the potential. Later in this paper [Table VII, column (e)], we quote matrix elements of the attractive part of the $^1S_0$ potential by itself. These are -9.05, -8.73, -7.64 MeV, respectively, for the $n=0$, 1, 2 matrix elements, respectively. This latter potential, $^1S_0(1)$ in Table I, possesses a range of $\sim$0.7 F. If we then employ a potential of range 1.4 F whose strength is adjusted to achieve equality with the previous $n=0$ matrix element, we find $n=1, 2$ matrix elements of -3.55 MeV and -2.48 MeV, respectively. This decrease with n does not occur for the shorter-range force, since at $r=0$ the relative wave function $R_{n0}(r)$ is an increasing function of n. The longer-range separable force can sense the decrease in magnitude and the nodes which occur for $r>0$. In this latter discussion, one must recall that for a separable potential radial integrals of the force appear as

$$\langle n0 \mid v \mid n0\rangle\sim\left(\int v(r)R_{n0}(r)r^2dr\right)^2,$$

whereas for a local force one has

$$\langle n0 \mid v \mid n0\rangle\sim\int v(r)R_{n0}^2(r)r^2dr.$$

In the limit of very long range for either force, one will clearly find a different behavior with n. Indeed, many of the disparities in the reference-spectrum matrix elements may be tied to the different nature of local and nonlocal forces.

IV. RESULTS AND DISCUSSION OF OSCILLATOR CALCULATIONS

It is possible to read the limiting values of $K_N(E)$ predicted by the reference-spectrum expansion from Figs. 11(a) and 11(b). A more complete listing of matrix elements of $K_N(E)$, obtained by direct solution of Eq. (24) for varying sizes of the gap Δ, is given in Table V.

In evaluating these matrix elements, an angle-averaged diagonal approximation for Q was employed, i.e.,

$$\langle nlNL \mid Q \mid n'l'N'L'\rangle=\delta_{NN'}\delta_{LL'}\delta_{ll'}[2l+1]^{-1}[2L+1]^{-1}\times\sum_{\Lambda=|L-l|}^{|L+l|}(2\Lambda+1)\langle nlNL,\Lambda \mid Q \mid nlNL,\Lambda\rangle, \quad (40)$$

TABLE IV. Comparison of some reference-spectrum matrix elements from the separable potential of Table I with those from the HJ potentials. The latter are taken from the work of Wong (Ref. 9). The matrix elements obtained from the local potential fall off somewhat more rapidly with increasing γ^2 and considerably more rapidly with increasing n.

		Separable potential (a)			Hamada-Johnston potential			Separable potential (b)		
					γ_n^2 (F^{-2})					
	n	1	2	3	1	2	3	1	2	3
$K(^3S_1)$	0	−15.40	−12.55	−11.57	−11.28	−7.69	−5.86	−13.9	−11.2	−10.0
(MeV)	1	−13.26	−10.82	−9.96	−7.49	−4.47	−2.72	−12.3	−9.9	−8.8
	2	−10.01	−8.14	−7.47	−3.01	−0.49	+0.71	−9.9	−7.9	−7.2
$K(^1S_0)$	0	−7.79	−7.07	−6.77	−7.05	−6.05	−5.43			
	1	−5.86	−5.31	−5.08	−4.54	−3.57	−2.87			
	2	−3.66	−3.28	−3.11	−1.51	−0.66	−0.06			

which, when combined with the relation

$$\sum_{\Lambda''} U(L''l''Js;\Lambda''j)U(L''l''Js;\Lambda''j'')=\delta_{jj''},$$

greatly simplifies Eq. (29). One notable consequence of Eq. (40) is the removal from Eq. (29) of any dependence on the total angular momentum J. For matrix elements of $K_N(E)$ in ^1S states, or ^3S states with $L=L'=0$, the angle averaging will not have any effect aside from eliminating coupling by other than the tensor force to states of higher relative angular momentum. As a numerical example of a matrix element which is affected by angle averaging one might consider the matrix element labelled by the relative and c.m. numbers (0012) and listed in the second row of Table V. This triplet-spin matrix element is associated with possible total angular momentum $J=1, 2, 3$. The spread we find about the average value quoted in Table V is some $\pm 2\%$. In a few smaller, and therefore less important, nuclear matrix elements the errors incurred by using the angle averaging approximation are as large as $\pm 5\%$.

We have also tried to indicate the consequences of the diagonal assumption for N included in Eq. (40). In Table VI, we have listed a few of the $^1S_0$ matrix elements calculated with and without the diagonal assumption. When the diagonal restriction was relaxed, we considered differences $|N-N'|$ as large as 30. Nevertheless, the two sets of matrix elements agree remarkably well. Our conclusions on the accuracy of the above approximations agree, of course, with similar statements by Wong.

Also included in Table V are the $\epsilon=-80$ MeV spectrum matrix elements for states other than shown in Figs. 11(a) and 11(b). It is clear that the expansion of $K_N(E)$ in terms of $K(\epsilon)$ is a very useful one for $\epsilon<0$. To achieve a good-state-independent approximation to the nuclear reaction matrix one must match the choice of ϵ to the size of Δ. For the gapless single-particle spectrum the selection $\epsilon=-80$ MeV is reasonable, while for $\Delta=94$ MeV ϵ must be decreased to -200 MeV. Independent of Δ, the convergence of $K(\epsilon)$ to $K_N(E)$ is particularly good in the region -60 MeV$<\epsilon<-200$ MeV, where inclusion of the quadratic term produces sufficient accuracy.

It is interesting to note that the so-called phase-shift method of Kallio[8] amounts to a use of the above expansion at the relative oscillator energy $\epsilon=\epsilon_{nl}=(2n+l+\frac{3}{2})\hbar\omega$. Some matrix elements obtained in this fashion are included in Table V. The discrepancies between our fit and the experimental phase shifts will be reflected to some extent in these phase-shift matrix elements. The values obtained for the $^1S_0$, $^3S_1$ states show the largest deviations from the exact matrix elements. The strong interaction in the s states perhaps negates the use of a phase-shift method in these states.[23]

It is, of course, of paramount interest to compare the matrices $K_N(E)$ obtained using different potentials v. First, one may stay within the framework provided by a separable potential and alter, say, the nature of the repulsive contribution to the potential or the strength of the tensor component in the $^3S_1$, $^3D_1$ states. In Table VII, we have presented the ^1S and $^3S_1$-$^3D_1$ nuclear matrix elements obtained using the Yamaguchi potential, the Tabakin potential, and our potentials possessing either finite or infinite hard cores. The Yamaguchi potential differs most from the other two in its inability to produce a weakening of the nuclear matrix elements with increasing number of relative nodes (n). This decrease in strength of the residual interaction is due presumably to the increased sensitivity of the states with larger n to high-energy repulsion in the force. As we have seen, one could also produce a similar drop off with n by employing a single-term attractive potential with a longer range. Such a separable force would not fit either the low- or high-energy data.

Also listed in Table VII are the matrix elements of

[23] D. Koltun, Phys. Rev. Letters 19, 910 (1967).

TABLE V. Matrix elements of $K^N(E)$ obtained from the separable potential specified in Table I and using a varying gap Δ in the oscillator single-particle spectrum. The gap of 94 MeV corresponds roughly to $\Delta=E_{sd}$. The $^3S_1$ matrix elements are listed for the potentials $^3S_1$ (a) and $^3S_1$ (b) as well as for a completely uncoupled $^3S_1$ potential. The purely S-state matrix elements are calculated with and without an infinite repulsive core. Also included in this table are the reference-spectrum matrix elements $\langle K(\epsilon)\rangle$ for the choice $\epsilon=-80$ MeV ($\gamma^2=2$ F^{-2}) and some phase-shift matrix elements $\langle K(\epsilon_{nl})\rangle$. These appear in columns (d) and (e), respectively. The reference choice $\epsilon=-80$ MeV is a good starting point for the expansion of the gapless $K_N(E)$. The choice $\epsilon=-200$ MeV would be reasonable for $\Delta=94$ MeV.

	n	l	n'	l'	N	L	(a) Δ (MeV) +0	(b) +47	(c) +94	(d) $\langle K(\epsilon)\rangle$ $\epsilon=-80$	(e) Phase shift
$^3S_1$-$^3D_1$	0	0			2	0	−13.66	−11.33	−10.56	−12.55	−20.9
					1	2	−13.30	−11.22	−10.50		
potential (a)					0	4	−13.12	−11.18	−10.53		
	1	0			1	0	−10.26	−9.12	−8.73	−10.82	−8.1
$P_D=0.32\%$					0	2	−10.32	−9.18	−8.78		
	2	0			0	0	−7.47	−6.73	−6.47	−8.14	−4.6
	1	0	0	2	1	0	−1.44	−1.33	−1.30	−1.56	−1.08
					0	2	−1.43	−1.33	−1.30		
	2	0	1	2	0	0	−1.52	−1.47	−1.45	−1.74	−1.05
	0	2			1	0	+1.67	1.85	1.95	1.90	
					0	2	1.67	1.85	1.95		
	1	2			0	0	2.61	2.94	3.12	3.06	
$^3S_1$-$^3D_1$	0	0			1	2	−13.00	−10.33	−9.46		
potential (b)	1	0			1	0	−10.49	−8.70	−8.07		
	2	0			0	0	−7.27	−6.88	−6.40		
$P_D=2.8\%$	0	2	1	0	1	0	−4.24	−3.91	−3.83		
	1	2	2	0	0	0	−4.24	−3.99	−3.95		
	0	2			1	0	1.35	1.68	1.83		
	1	2			0	0	1.88	2.32	2.53		
$^1P_1$	0	1			1	1	1.53	1.64	1.71	1.67	1.39
					0	3	1.53	1.64	1.71		
	1	1			0	1	2.54	2.90	3.17	3.20	2.32
$^3D_2$	0	2			1	0	−2.69	−2.46	−2.36	−2.42	
					0	2	−2.69	−2.46	−2.36		
	1	2			0	0	−3.73	−3.35	−3.20	−3.25	
$^3D_3$	0	2			1	0	−0.12	−0.12	−0.12	−0.12	−0.12
					0	2	−0.12	−0.12	−0.12		
	1	2			0	0	−0.30	−0.30	−0.29	−0.29	−0.29
$^1S_0$	0	0			2	0	−7.17	−6.63	−6.43	−7.07	−8.2
$g_2<\infty$					1	2	−7.11	−6.60	−6.41		
					0	4	−7.04	−6.57	−6.34		

TABLE V (*Continued*)

	n	l	n'	l'	N	L	(a) +0	(b) Δ (MeV) +47	(c) +94	(d) $\langle K(\epsilon)\rangle$ $\epsilon=-80$	(e) Phase shift
	1	0			1	0	−5.07	−4.83	−4.73	−5.31	−4.1
					0	2	−5.05	−4.82	−4.73		
	2	0			0	0	−3.08	−2.96	−2.90	−3.28	−2.3
$^1S_0$	0	0			2	0	−7.16	−6.61	−6.40		
					1	2	−7.09	−6.58	−6.38		
$g_2=\infty$					0	4	−7.02	−6.56	−6.36		
	1	0			1	0	−5.05	−4.81	−4.68		
					0	2	−5.03	−4.80	−4.67		
	2	0			0	0	−3.06	−2.93	−2.83		
$^3P_0$	0	1			1	1	−2.11	−2.05	−2.03	−2.08	
					0	3	−2.10	−2.05	−2.03		
	1	1			0	1	−1.46	−1.44	−1.44	−1.49	
$^3P_1$	0	1			1	1	1.76	1.88	1.95	1.89	
					0	3	1.77	1.88	1.75		
	1	1			0	1	2.59	2.81	2.94	2.86	
$^3P_2$	0	1			1	1	−1.07	−1.01	−0.99	−1.00	
					0	3	−1.07	−1.01	−0.99		
	1	1			0	1	−1.85	−1.73	−1.68	−1.69	
$^1D_2$	0	2			1	0	−0.50	−0.49	−0.48	−0.48	
					0	2	−0.51	−0.49	−0.48		
	1	2			0	0	−0.88	−0.85	−0.84	−0.84	
uncoupled $^3S_1$	0	0			2	0	−13.92	−11.56	−10.80		
					1	2	−13.63	−11.45	−10.83		
					0	4	−13.34	−11.37	−10.69		
$g_2<\infty$	1	0			1	0	−10.78	−9.53	−9.07		
					0	2	−10.60	−9.50	−9.05		
	2	0			0	0	−7.54	−6.82	−6.51		
uncoupled $^3S_1$	0	0			2	0	−13.58	−11.34	−10.62		
					1	2	−13.31	−11.24	−10.56		
					0	4	−13.05	−11.16	−10.51		
$g_2=\infty$	1	0			1	0	−10.51	−9.32	−8.89		
					0	2	−10.40	−9.29	−8.87		
	2	0			0	0	−7.42	−6.72	−6.44		

TABLE VI. Comparison of $^1S_0$ matrix elements obtained (a) in a diagonal approximation for Q, (b) for nonzero diagonal and off-diagonal matrix elements of Q. Off-diagonal matrix elements of $K_N(E)$ can be nonvanishing only if Q is allowed to be nondiagonal.

n	l	N	L	n'	l'	N'	L'	J	(a)	(b)
0	0	2	0	0	0	2	0	0	−7.17	−7.20
1	0	1	0	1	0	1	0	0	−5.07	−5.08
2	0	2	0	2	0	2	0	0	−3.08	−3.00
1	0	0	2	0	0	1	2	2	0	0.19
1	0	1	0	0	0	2	0	0	0	0.10

the Tabakin potential and of our finite core potential. The repulsive component of the force clearly plays a more influential role for our potentials. Among those states not explicitly shown in Table VII, a notable difference occurs for the $^3D_3$ matrix elements for which the Tabakin potential gives −0.69 and −1.04 MeV for the $n=0, 1$ states, respectively. Finally, it is evident that the use of an infinite, rather than a finite, repulsive core with the separable potentials produces only minor changes in nuclear matrix elements relevant to the shell model.

A second and important feature we have suggested varying in the separable potential is the strength of the tensor force. An adequate fit to the $^3S_1$-$^3D_1$ coupling parameter ρ does not guarantee a reasonable depth for the tensor force. A more accurate measure of this component of the force would appear to be the deuteron D-state probability. In Table VIII, we have presented $^3S_1$-$^3D_1$ nuclear reaction matrix elements for separable forces with varying degree of tensor strength. We have included in this table matrix elements for the Yamaguchi-Yamaguchi[12] coupled $^3S_1$-$^3D_1$ potential as well as for the potentials considered in Table VII.

For zero gap in the single-particle oscillator spectrum, the purely S-wave reaction matrix elements obtained from the many potentials are nearly equal. The only exceptions occur for the Tabakin matrix elements, which are appreciably smaller than those deduced from the other potentials. This diminished S-wave strength can probably be attributed to the failure of the Tabakin potential to fit the $^3S_1$ scattering length. Experimentally this parameter is 5.44 F in contrast to the Tabakin value of 7.1 F. Despite the above-noted similarity between S-wave gapless matrix elements, the $^3S_1$-$^3D_1$ coupling matrix elements differ markedly. These matrix elements, as might be expected, are largest for our $^3S_1$-$^3D_1$ potential (b) and for the coupled Yamaguchi-Yamaguchi potential. The latter potential yields a D-state probability of only 4%, but contains no repulsion in any of the states in which it acts. The coupling matrix elements obtained from our potential (a) are small, while those from the uncoupled Yamaguchi potential vanish.

However, when one turns on a finite gap in the single-particle spectrum, the influence of the tensor force is

TABLE VII. Comparison of nuclear matrix elements for separable potentials containing varying degrees of repulsion. In this calculation we set $\Delta=0$ and $\hbar\omega=13.4$ MeV. Matrix elements from the S-state potential obtained using the form factors in Eqs. (4) and (6) are shown in column (a) with g_2 finite and in column (b) with $g_2=\infty$. Matrix elements from an uncoupled version of the $^3S_1$ potential are also shown. The Tabakin and Yamaguchi matrix elements appear in columns (c) and (d), respectively. First-order perturbation theory values of the attractive and repulsive parts of the $^1S_0$ potential used in (a) are indicated separately in (d) and (f). Corresponding perturbation values for the Tabakin potential are listed in (g) and (h).

	n	l	n'	l'	N	L	J	$\langle \lvert K_N \rvert \rangle$ (a) $g_2<\infty$	(b) $g_2=\infty$	(c) Tabakin	(d) Yamaguchi	$\langle \lvert v \rvert \rangle$ (e)	(f)	(g)	(h)
$^1S_0$	0	0			2	0	0	−7.17	−7.16	−7.20	−7.54	−9.05	4.49	−5.91	0.58
	1	0			1	0	0	−5.07	−5.05	−4.74	−6.05	−8.73	6.63	−4.71	0.44
	2	0			0	0	0	−3.08	−3.06	−2.67	−4.83	−7.64	8.09	−3.72	1.16
S_1-$^3D_1$	0	0			1	2	1	−13.39		−11.71	−13.30				
	1	0			1	0	1	−10.26		−9.23	−11.73				
	2	0			0	0	1	−7.47		−7.30	−10.09				
	0	2	1	0	1	0	1	−1.44		−2.06					
	1	2	2	0	0	0	1	−1.52		−2.25					
	0	2			1	0	1	1.67		3.35					
	1	2			0	0	1	2.61		3.15					
$^3S_1$ uncoupled	0	0			2	0	1	−13.92	−13.58						
	1	0			1	0	1	−10.78	−10.51						
	2	0			0	0	1	−7.54	−7.42						

TABLE VIII. Comparison of the $^3S_1$-$^3D_1$ matrix elements of potentials possessing varying amounts of tensor force. In this comparison we employ a vanishing gap in the oscillator spectrum and consider our $^3S_1$ (a) and (b) potentials as well as the potentials of Yamaguchi (Y) and Yamaguchi-Yamaguchi (YY).

	n	l	n'	l'	N	L	$K_N(E)$ for $\Delta=0$ (MeV) $^3S_1$ (a)	$^3S_1$ (b)	Y	YY
$^3S_1$	0	0			1	2	−13.30	−13.00	−13.30	−13.31
	1	0			1	0	−10.26	−10.49	−11.73	−11.22
	2	0			0	0	−7.47	−8.27	−10.09	−9.78
$^3S_1$-$^3D_1$	0	2	1	0	1	0	−1.44	−4.24	0	−4.96
	1	2	2	0	0	0	−1.52	−4.24	0	−6.19
$^3D_1$	0	2			1	0	1.07	1.35	0	−2.22
	1	2			0	0	2.61	1.88	0	−3.96

felt even in the purely S-wave matrix elements. This information is contained in Table V, where matrix elements of our potentials (a) and (b) are given for $\Delta=94$ MeV. Clearly, the matrix elements of both potentials are diminished in magnitude by the introduction of a gap, but the reduction in size is greatest for the potential possessing the larger tensor component. This behavior has been observed previously in nuclear matter computations by many authors and in finite nuclear reaction matrix calculations by Wong.[1] The classic argument presented to explain this tensor quenching states that the tensor force which contributes to the S-wave interaction through a second Born approximation does so less effectively inside a nucleus than in free space. The interactions which occur within the nucleus are off the two-body energy shell and, evidently, the second-order tensor force decreases appreciably in such a situation. What we have demonstrated is that, at least for separable potentials, the amount of quenching which is obtained is quite dependent on the gap in the single-particle spectrum. We will return to this point in Sec. V, where plane-wave intermediate states will be discussed.

Finally, we would like to comment more generally on the effect on two-body matrix elements of introducing a gap into the oscillator spectrum, (indicated in Table V). Those matrix elements which show a more marked dependence on ϵ when calculated to lowest order in $K(\epsilon)$ are understandably most influenced by the gap. When Δ is increased from 0 to 94 MeV the $n=0$ $^3S_1$ reaction matrix elements arising from potentials (a) and (b) suffer reductions of 23 to 30%, respectively. Clearly, larger bounds for this reaction matrix element result from uncertainties in one's knowledge of the single-particle spectrum, rather than uncertainties in the size of the tensor force. Some understanding of the Δ dependence of a particular matrix element can be obtained from perturbation theory. Clearly, any dependence on Δ can first enter a reaction matrix element in the energy denominator of the second-order Born term. Thus, matrix elements for states in which the force is attractive will decrease in magnitude, and those for states with repulsive forces increase in magnitude, when Δ is increased. Also, states in which the force is especially weak will exhibit little dependence on Δ.

In concluding this section, it is appropriate to refer to the work of McCarthy,[10] who has extracted reaction matrix elements from Eq. (24) using the HJ potential and oscillator wave functions for all single-particle states. In Figs. 14 and 15, we have displayed the behavior with Δ of the $^3S_1$ (b) and $^1S_0$ diagonal matrix elements taken from Table V and from McCarthy's

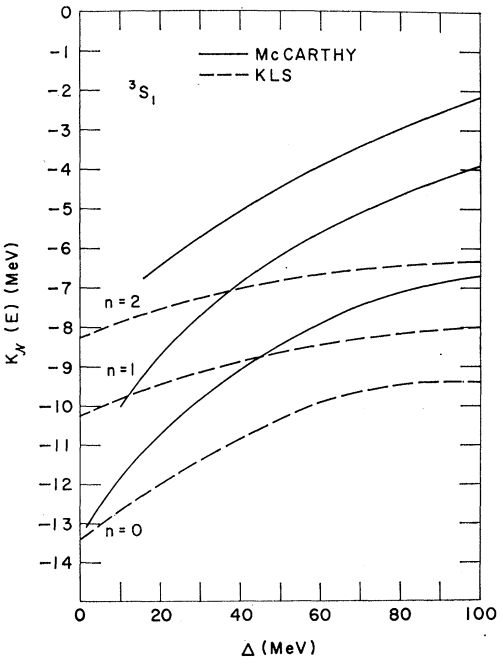

FIG. 14. Comparison of the $^3S_1$ reaction matrix elements from our separable potential $^3S_1$ (b) with those obtained by McCarthy (Ref. 10) from the HJ potential. The dependence of these matrix elements on the gap in the oscillator spectrum Δ is shown. We should point out that McCarthy used a slightly larger oscillator parameter $\hbar\omega=14$ MeV. The qualitative conclusions to be drawn from this diagram are not altered, however.

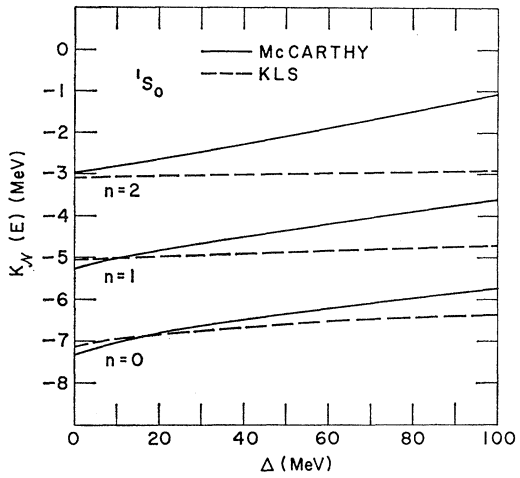

FIG. 15. Comparison of the $^1S_0$ reaction matrix elements from our separable potential with those obtained by McCarthy (Ref. 10) from the HJ potential.

calculation. The two sets of matrix elements are not strictly comparable, since McCarthy used an oscillator parameter $\hbar\omega=14$ MeV, whereas we have $\hbar\omega=13.4$ MeV. The qualitative features of the comparison we are presenting will not be greatly altered if this minor adjustment is made. The local and nonlocal potentials yield matrix elements which are surprisingly similar for a small gap in the oscillator spectrum but which begin to diverge as the gap size is increased. The HJ matrix elements drop off more quickly with increasing Δ, presumably mirroring the comparable behavior with ϵ observed in the corresponding reference-spectrum matrices. The McCarthy results provide striking confirmation of our contention that the gapless $^3S_1$ reaction matrix elements are unaffected by the amount of tensor force in the underlying potentials.

V. PLANE-WAVE INTERMEDIATE STATES

The final component of our calculations which we would like to alter is the shell-model Hamiltonian H_0. To permit a more direct and meaningful comparison with the results of Wong[9] for the local HJ potential, we will now use, with our potential, a set of plane-wave intermediate states. We retain the oscillator description for the occupied states in the $1s$, $1p$, $2s$-$1d$ shells and orthogonalize the plane-wave particle states to these hole states. Specifically, we will rewrite the propagator in Eq. (24) as

$$Q[1/(E'-T)]Q, \tag{41}$$

where $T=T(1)+T(2)=t+T_{\text{c.m.}}$ is the total kinetic energy of a nucleon pair and E' as given in Eq. (25). There is some doubt whether one should use the kinetic-energy operator T or an operator like QTQ which commutes with Q in the energy denominator in (41).[24] We will discuss the relevance of this view later. We will simplify our calculations by making the assumption that Q is completely diagonal. Thus, our results will correspond to those obtained in the $GA(0)$ treatment of Wong. Our earlier discussion of the effect of a diagonal assumption on ^1S matrix elements and the small variations seen between Wong's $GA(0)$ and $GA(2)$ results attest to the accuracy of this assumption. It is interesting that for oscillator intermediate states one can write

$$Q/(E-H_0)=Q[1/(E-H_0)]Q, \tag{42}$$

provided one treats both sides of this equation exactly. If, however, one assumes that Q is a diagonal operator, then the existence of matrix elements of Q which are less than unity leads to a reduction in the right-hand side of Eq. (42) relative to the left-hand side. It is a simple matter to check the extent of this reduction. The $^3S_1$, $n=0$ matrix elements which are most effected by a diagonal approximation in Eq. (42) are reduced approximately 10% when a vanishing gap is used in the oscillator spectrum. When the gap in the oscillator spectrum is increased to 47 or 94 MeV one finds a very small decrease in all matrix elements. If (as one might expect) the plane-wave states are better represented by oscillator states with an appreciable gap, then we can probably trust the diagonal restriction placed on Q in the propagator (41).

To carry out the plane-wave intermediate-state calculation along the lines of Sec. IV, only the matrix elements

$$\langle nlNL \mid Q[1/(E'-T)]Q \mid n'l'N'L'\rangle$$

need be reevaluated. This requires the calculation o matrix elements

$$\langle nlNL \mid Q[1/(E'-T)]Q \mid n'l'N'L'\rangle, \tag{43}$$

which are given schematically for uncoupled s states by

$$\sum_{n'',n'''}\langle nlNL \mid Q \mid n''lN''L\rangle \int k^2dk\, P^2dP\, R_{n''l}(k) \times R_{n'''l}(k)R_{N''L}(P)R_{N'''L}(P)[E'-(\hbar^2/m)(k^2+\tfrac{1}{4}P^2)]^{-1} \times\langle n'''lN'''L \mid Q \mid nlNL\rangle. \tag{44}$$

Further, we write

$$Q[1/(E'-T)]Q=(Q-1)[1/(E'-T)](Q-1) +(Q-1)[1/(E'-T)]+[1/(E'-T)](Q-1) +[1/(E'-T)]. \tag{45}$$

[24] See, for example, M. Baranger (Ref. 1). An alternative viewpoint could be based on the observation that "particle" states lie in the continuum. Their spectrum is then just that obtained from the kinetic energy operator. However, their wave functions would be distorted by any potential interaction with the nuclear core. One might then ask to what extent the particle-state wave functions are approximated by plane waves orthogonalized to the occupied states.

The first three terms on the right-hand side of Eq. (45) may be treated as indicated in Eq. (44), since their contributions from the summations cut off when the total oscillator quantum number in the summed states exceeds a reasonably low value. The final term in Eq. (45) is the propagator one would expect were the exclusion principle inoperative. The contribution of this last term to an uncoupled matrix element $\langle nlNL \mid \pi_N{}^{ii'}(E) \mid n'l'N'L' \rangle$ is

$$\sum_{n''} \int k^2dk \int P^2dP\, v_l{}^i(k) R_{n''l}(k) R_{NL}(P) R_{N'L}(P) \times [E-(\hbar^2/m)(k^2+\tfrac{1}{4}P^2)]v^{i'}(n''l) = \int P^2dP\, R_{NL}(P) R_{N'L}(P) \int k^2dk\, v_l{}^i(k) v_l{}^{i'}(k) \times [E-(\hbar^2/m)(k^2+\tfrac{1}{4}P^2)]^{-1}. \quad (46)$$

In treating plane-wave intermediate states, one might wish to use as a reference reaction matrix the solution of

$$K_T(\tilde{E}) = v + v[1/(\tilde{E}-T)]K_T(\tilde{E}). \quad (47)$$

If one takes matrix elements of this latter equation in plane-wave c.m. states, one obtains

$$\langle P \mid K_T(\tilde{E}) \mid P \rangle = v + v \frac{1}{\tilde{E}-(\hbar^2P^2/4m)-t} \times \langle P \mid K_T(\tilde{E}) \mid P \rangle, \quad (48)$$

and, hence concludes that

$$\langle P \mid K_T(\tilde{E}) \mid P \rangle = K(\tilde{E}-\hbar^2P^2/4m). \quad (49)$$

Nuclear matrix elements are then obtained by averaging over the corresponding free-reaction matrix elements in the fashion[25]

$$\langle nlNL \mid K_T(\tilde{E}) \mid n'lN'L \rangle = \int P^2dP\, R_{NL}(P) R_{N'L}(P) \times \langle nl \mid K(\tilde{E}-\hbar^2P^2/4m) \mid n'l \rangle. \quad (50)$$

In Table IX, we have presented the $K_N(E)$ matrix elements deduced using our form of the separable potential and the procedure described in this section. For comparison, we also list the corresponding matrix elements obtained by Wong in the approximation $GA(0)$, and a few of the matrix elements of $K_T(E)$.

If one's point of reference is the gapless oscillator calculation of $K_N(E)$, then one must conclude a substantial but not radical change is produced in $K_N(E)$ by the substitution of plane wave for oscillator intermediate states. However, the introduction of a gap into the oscillator spectrum simulates many of the changes wrought by plane waves. The matrix elements most affected by the substitution are those for the ${}^3S_1$ states in which the force is strongest. For the ${}^3S_1$ states with $n=0$, $l=0$ the diagonal matrix elements obtained with no gap in the oscillator spectrum are reduced by some 30% when a plane-wave spectrum is employed. This reduction is reproduced by using an oscillator gap of approximately 90 MeV. A crude but intuitively appealing argument suggests that to recover the plane-wave results from an oscillator basis one should employ a state-dependent gap. If in solving for the nuclear reaction matrix we assume Q is diagonal in the c.m. coordinates, then we may write $(E-H_0)^{-1} \approx (E-E_{NL}-t-u)^{-1}$, for the oscillator case where E_{NL} is the oscillator c.m. energy and u the oscillator relative potential energy. With the further, and not as well founded, assumption of c.m. diagonality for T, we have in the case of plane waves

$$(E'-T)^{-1} \approx (E'-\tfrac{1}{2}E_{NL}-t)^{-1}.$$

One can easily argue that the relative potential energy, because of the short range of the nuclear force, is small in all situations which we consider.[24] To make the above two propagators agree, then, one should take $E = E'+E_{sd}-\Delta = E'+E_{sd}-(E_{sd}-\frac{1}{2}E_{NL})$, thus introducing the state-dependent gap

$$\Delta_{NL} = 7\hbar\omega - \tfrac{1}{2}(2N+L+\tfrac{3}{2})\hbar\omega.$$

If one were to obtain the plane-wave reaction matrix elements by interpolation from Table V, it may be argued that a slight improvement in accuracy results from the use of Δ_{NL}, rather than the state-independent value $\Delta=94$ MeV. However, it is of crucial importance to use the above state-dependent gap in comparing the plane-wave results of Wong[9] with the oscillator calculation of McCarthy. The HJ reaction matrix is far more sensitive to changes in Δ.

One may note parenthetically that the use of (47) as a reference matrix in the plane-wave situation is particularly bad for the ${}^3S_1$, $n=2$ matrix element. If one used $K_T(\tilde{E})$ with $\tilde{E}=E'=-13$ MeV, then one could expect a Pauli correction $\sim$6 MeV in this state. The averaging in Eq. (50) takes one, for the $n=1$, 2 states, uncomfortably close to the deuteron pole in $K(\epsilon)$. A better state-independent reference matrix to employ is then the free reaction matrix $K(\epsilon)$, with ϵ having some negative value reasonably far removed from the bound-state singularity. The value $\epsilon=-200$ MeV is a good choice for the previous plane-wave calculation. We recall that for the separable potentials the gapless oscillator matrix elements were reasonably well approximated by $K(\epsilon)$ at $\epsilon=-70$ to -80 MeV, but that the $\Delta=94$-MeV oscillator elements would have required $\epsilon\sim-200$ MeV.

[25] One might well have guessed that the matrix elements in Eq. (50) could be approximated by

$$\langle nlNL \mid K_T(E') \mid n'lNL \rangle = \langle nl \mid K(E'-\alpha E_{NL}) \mid n'l \rangle$$

with $\alpha=\frac{1}{2}$. In practice, we found this approximation, which could also be used in evaluating the c.m. integral in Eq. (43), to be improved by the choice $\alpha=0.4$.

TABLE IX. Nuclear reaction matrix elements using plane waves for intermediate states. The form of the propagator is varied as indicated in the column headings. All plane-wave calculations are carried out in an angle-averaged diagonal approximation for the operator Q'. We took $\hbar\omega=13.4$ MeV and $E'=-13$ MeV. Also we used only S-wave potentials possessing infinite cores. $GA(0)$ results of Wong (Ref. 9), which are included in the last column for comparison, were obtained using $E'=-8$ MeV and $\hbar\omega=13.5$ MeV'. All matrix elements are listed in MeV.

	n	l	n'	l'	N	L	(a) $\frac{1}{E'-T}$	(b) $\frac{1}{E'-QTQ}$	(c) $\frac{1}{E'-T}$	(d) Wong
$^3S_1$-$^3D_1$										
	0	0			2	0	−10.73	−11.28	−15.43	
potential (a)					1	2	−10.58	−11.07	−15.16	−8.85
					0	4	−10.47	−10.85	−14.66	
	1	0			1	0	−8.76	−9.03	−14.53	−6.12
					0	2	−8.72	−8.92	−14.60	
	2	0			0	0	−6.52	−6.65	−12.96	−3.32
	1	0	0	2	1	0	−1.31	−1.33	−2.00	−3.11
					0	2	−1.30	−1.32	−1.94	
	2	0	1	2	0	0	−1.45	−1.47	−2.51	−3.63
	0	2			1	0	1.97	1.93	1.73	1.24
					0	2	1.97	1.93	1.74	
	1	2			0	0	3.72	3.08	2.68	1.63
$^3S_1$-$^3D_1$	0	0			1	2	−9.49			
	1	0			1	0	−7.99			
potential (b)	2	0			0	0	6.43			
	0	2	1	0	1	0	−3.82			
	1	2	2	0	0	0	−3.96			
	0	2			1	0	1.85			
	1	2			0	0	2.52			
$^1P_1$	0	1			1	1	1.70	1.67		
					0	3	1.71	1.68		
	1	1			0	1	3.17	3.12		
$^3D_2$	0	2			1	0	−2.37	−2.40		
					0	2	−2.38	−2.41		
	1	2			0	0	−3.21	−3.24		
$^3D_3$	0	2			1	0	−0.12	−0.12		
					0	2	−0.12	−0.12		
	1	2			0	0	−0.29	−0.29		
$^1S_0$	0	0			2	0	−6.48	−6.63	−7.81	−6.49
					1	2	−6.43	−6.58	−7.74	−6.50
					0	4	−6.39	−6.50	−7.61	−6.41
	1	0			1	0	−4.75	−4.81	−6.12	−4.23
					0	2	−4.73	−4.78	−6.03	
	2	0			0	0	−2.92	−2.94	−4.15	−1.77

TABLE IX (*Continued*)

	n	l	n'	l'	N	L	(a) $Q\frac{1}{E-T}Q$	(b) $Q\frac{1}{E-QTQ}Q$	(c) $\frac{1}{E-T}$	(d) Wong
$^3P_0$	0	1			1	1	−2.03	−2.05		
					0	3	−2.02	−2.04		
	1	1			0	1	−1.44	−1.44		
$^3P_1$	0	1			1	1	1.94	1.91		
					0	3	1.95	1.92		
	1	1			0	1	2.94	2.90		
$^3P_3$	0	1			1	1	−0.99	−1.00		
					0	3	−0.99	−1.00		
	1	1			0	1	−1.68	−1.69		
$^1D_2$	0	2			1	0	−0.48	−0.49		
					0	2	−0.48	−0.49		
	1	2			0	0	−0.84	−0.84		

Since the suitability of the propagator (41) cannot be easily justified, we have also investigated a previously mentioned alternative[24]:

$$Q(E'-QTQ)^{-1}Q=Q(E'-T)^{-1}Q+Q(E'-T)^{-1}(QTQ-T)(E'-T)^{-1}Q+\cdots. \quad (51)$$

We have retained only the first two terms in the right-hand side of Eq. (51). Because of the positive definite nature of the kinetic energy operator, one might expect the matrix elements of the propagator of Eq. (51) to be larger than those of Eq. (41), and, consequently, the residual interaction in, say, the $^3S_1$ and $^1S_0$ states to be more attractive. The matrix elements of $K_N(E')$, obtained using (51) and shown in Column (b) of Table IX, bear out this expectation and testify to the relative accuracy of the propagator (41)—if one views (51) as a more logical choice. Including the omitted terms in our treatment of the propagator (51) would not lead to a substantial increase in the attractive residual interaction matrix elements.

In place of the expansion indicated in Eq. (51), one might have written

$$Q(E'-QTQ)^{-1}Q=Q(E'-QTQ)^{-1}=Q(E'-T)^{-1}+Q(E'-T)^{-1}(QTQ-T)(E'-T)^{-1}+\cdots. \quad (52)$$

The discussion associated with Eq. (42) suggests that the diagonal assumption for Q is better coupled with the expansion (52) than with (51). Indeed, a literal reading of Wong's paper[9] leads one to beieve he used as a propagator $Q(E'-T)^{-1}$ rather than (41).

In view of the markedly different behavior of the reference-spectrum diagonal matrix elements obtained by Wong from the Hamada-Johnston potential or by us from a separable potential, one is not surprised by some disagreement between the corresponding plane-wave reaction matrix elements. However, the largest differences which are obtained in the $^3S_1$ matrix elements, are not large as one might have predicted from Fig. (14). The greater sensitivity of the HJ reaction matrix to Δ, apparent when one uses oscillator intermediate states, does not result in drastically altered plane-wave matrix elements. Indeed, if one uses the reaction matrix deduced from our potential (b), which possesses a tensor strength comparable to that in the HJ potential, then one finds the local and nonlocal $^3S_1$ $n=0$ matrix elements differ by only 6%. However, the more rapid decrease with n observed for the purely oscillator based HJ $^3S_1$ reaction matrix persists even when plane-wave intermediate states are employed.

Finally, we have in Table X, presented for comparison the $^3S_1$-$^3D_1$ reaction matrix elements deduced using plane-wave intermediate states, specifically the propagator $Q(E'-T)^{-1}Q$, and a variety of potentials. Our purpose here is, as in Sec. IV, to determine the role of the tensor force in these matrix elements. The HJ, Yamaguchi-Yamaguchi, and our potential (b) yield the smallest $^3S_1$, $n=0$ matrix elements and the largest $^3S_1$-$^3D_1$ matrix elements. The $^3S_1$, $n=0$ reaction matrix elements from the Yamaguchi potential or from our potential (a) are some 10% larger than for these latter three potentials.

The evidence extracted from our plane-wave calculation serves to enhance conclusions we have drawn in Sec. IV. The contribution of the tensor force to the $^3S_1$ reaction matrix elements is quenched either in the

TABLE X. Comparison of the $^3S_1$-$^3D_1$ reaction matrix elements obtained using plane-wave intermediate states, i.e., the propagator $Q(E-T)^{-1}Q$, and the potentials $^3S_1$-$^3D_1$, (a) and (b) of Kahana, Lee, and Scott, as well as the potentials of Tabakin (T), Yamaguchi (Y), Yamaguchi-Yamaguchi (YY), and Hamada-Johnston (HJ). Reaction matrix elements are given in MeV.

						$^3S_1$					
n	l	n'	l'	N	L	$^3S_1$ (a)	$^3S_1$ (b)	T	Y	YY	HJ
0	0			1	2	−10.58	−9.49	−9.04	−10.20	−9.08	−8.85
1	0			1	0	−8.76	−7.99	−7.45	−9.11	−7.67	−6.12
2	0			0	0	−6.52	−6.43	−6.00	−7.88	−6.46	−3.33
1	0	0	2	1	0	−1.31	−3.82	−2.15		−3.38	−3.11
2	0	1	2	0	0	−1.45	−3.96	−2.27		−4.08	−3.63
0	2			1	0	+1.97	1.85	3.78		−1.51	1.24
1	2			0	0	3.12	2.52	3.58		−2.62	1.63

presence of a gap in the oscillator spectrum or when plane waves are used for particle states. The degree of quenching does not seem to be strongly related to the range of the tensor force. However, the different dependence on the numbers of relative nodes n exhibited by the local and nonlocal reaction matrices is perhaps explained by the disparity in ranges of the underlying potentials.

VI. SUMMARY

We have used a variety of nonlocal potentials to study the finite nuclear residual interaction. The simple nature of our potentials enabled us to perform essentially exact calculations of the Brueckner reaction matrix. By restricting ourselves to the class of separable potentials were able to demonstrate that account must be taken of the high-energy scattering data which manifests itself most clearly in a quenching of the residual interaction in states with increasing numbers of relative nodes. The manner in which the high-energy data are fitted is of less importance. The Tabakin potential with its rather weaker repulsive core led to a $^1S_0$ residual interaction quite similar to that deduced from our potentials. Whether one used a finite or infinite repulsive core in our potential is of no consequence to the interaction between valence particles. Unfortunately, these conclusions are not necessarily valid for local potentials.

It was also a straightforward task to evaluate the accuracy of many commonly used approximations. In the purely oscillator calculations, for example, we found the assumption of a Q operator diagonal in c.m. quantum numbers to be good, desipte the existence of some fairly large off-diagonal matrix elements of Q. In addition, it was clear that the free reaction matrix $K(\epsilon)$ provides one with a quantitatively accurate reference matrix for a judicious choice of $\epsilon<0$. Of course, these judgements have been previously arrived at by Wong.[9] We did find one observation pertinent to plane-wave calculations. If the intermediate state Hamiltonian is chosen to be QTQ rather than T, then one may expect a rather stronger residual interaction in the $^3S_1$ states Clearly this point, as well as the more general question of propagation in particle states, require further study.

Finally, we compare the separable potential with the Hamada-Johnston potential. Perhaps the most important question to be answered in this comparison concerns the latitude resulting in the final nuclear reaction matrices from uncertainties in the tensor force and in the wave functions and spectrum to be used for intermediate states. When the gapless harmonic-oscillator spectrum was combined with any potential which gives an adequate fit to the purely $^3S_1$-wave data, the resulting reaction matrix elements were remarkably similar. Thus, the $\Delta=0$, $^3S_1$ reaction matrix elements of both our potentials $^3S_1$ (a), $^3S_1$ (b) and the HJ potential agree quite well. When a finite gap Δ is introduced between the valence and unoccupied levels (or when plane-wave intermediate states are used), one finds, understandably, that attractive reaction matrix elements are quenched while repulsive elements grow. When opposed to the 23% reduction for the $^3S_1$ (a) matrix element, the 30% diminuition in magnitude for the $^3S_1$ (b) reaction matrix element (obtained by replacing the gapless oscillator by a plane-wave spectrum) suggests that the presence of a tensor force enhances this quenching. Despite the obviously different dependences of the local and nonlocal reference spectrum matrices on ϵ or nuclear reaction matrices on Δ, the $n=0$, $^3S_1$ reaction matrix elements of the $^3S_1$ (b) potential or of the HJ potential differ by only 6%. The HJ $^3S_1$, $n=1, 2$ reaction matrix elements are, however, considerably less attractive than their nonlocal counterparts. We tended to ascribe this heightened n dependence of the HJ reaction matrix to the longer ranges present in the local force. A similar, but weakened, behavior may be observed in the $^1S_0$ states.

If, as seems likely, the plane-wave description of unoccupied states and the stronger tensor force are to be preferred, then one must conclude that the nuclear reaction matrix to be used as a bare residual interaction in finite nuclei is quite well defined. In addition, our

TABLE XI. The various functions $\pi_l^{ii'}=p\int_0^\infty q^2dq\, v_l^i(q)v_l^{i'}(q)[\epsilon-(\hbar^2/m)q^2]^{-1}$.

State	v_1	v_2	$\pi(\epsilon)$	
		(i) $\epsilon>0$		
$^1S_0$, $^3S_1$	$1/(k^2+a_1^2)$	$1/(k^2+a_2^2)$	$\pi_0^{ii}=-\pi(\epsilon_i-\epsilon)/4a_i(\epsilon_i+\epsilon)^2$	(A1)
			$\pi_0^{12}=-\pi(\epsilon_1\epsilon_2-\epsilon)/2(a_1+a_2)(\epsilon_1+\epsilon)(\epsilon_2+\epsilon)$	(A2)
$^3D_1$	$k^2/(k^2+a_1^2)^2$	$k^2/(k^2+a_2^2)^2$	$\pi_2^{ii}=-[\pi/32a_i(\epsilon_i+\epsilon)^4]\times(\epsilon_i^3+5\epsilon_i^2\epsilon+15\epsilon_i\epsilon^2-5\epsilon^3)$	(A3)
			$\pi_2^{12}=-[\pi/4(a_1+a_2)^3(\epsilon_1+\epsilon)^2(\epsilon_2+\epsilon)^2]\times\{\epsilon_1^2\epsilon_2^2+\epsilon_1\epsilon_2[2\epsilon_1+(\epsilon_1\epsilon_2)^{1/2}+2\epsilon_2]\epsilon+[\epsilon_1^2+3(\epsilon_1\epsilon_2)^{1/2}(\epsilon_1+\epsilon_2)+7\epsilon_1\epsilon_2+\epsilon_2^2]\epsilon^2-[\epsilon_1+3(\epsilon_1\epsilon_2)^{1/2}+\epsilon_2]\epsilon^3\}$	(A4)
$^1P_1$, $^3P_{0,1,2}$	$k/(k^2+a^2)^{3/2}$	$k^3/(k^2+a^2)^{5/2}$	$\pi_1^{11}=-\pi(\epsilon_a^2+6\epsilon_a\epsilon-3\epsilon^2)/16a(\epsilon_a+\epsilon)^3$	(A5)
			$\pi_1^{12}=-[\pi/32a(\epsilon_a+\epsilon)^4](\epsilon_a^3+5\epsilon_a^2\epsilon+15\epsilon_a\epsilon^2-5\epsilon^3)$	
			$\pi_1^{22}=-[\pi/256a(\epsilon_a+\epsilon)^5]\times(5\epsilon_a^4+28\epsilon_a^3\epsilon+70\epsilon_a^2\epsilon^2+140\epsilon_a\epsilon^3-35\epsilon^4)$	(A6)
$^1D_1$, $^3D_{2,3}$	$k^2/(k^2+a^2)^2$	$k^4/(k^2+a^2)^3$	$\pi_2^{11}=-[\pi/32a(\epsilon_a+\epsilon)^4]\times(\epsilon_a^3+5\epsilon_a^2\epsilon+15\epsilon_a\epsilon^2-5\epsilon^3)$	
			$\pi_2^{12}=$ Eq. (A6)	
			$\pi_2^{22}=-[\pi/512a(\epsilon_a+\epsilon)^6]\times(7\epsilon_a^5+45\epsilon_a^4\epsilon+126\epsilon_a^3\epsilon^2+210\epsilon_a^2\epsilon^3+315\epsilon_a\epsilon^4-63\epsilon^5)$	(A7)
		(ii) $\epsilon\equiv-\lambda\alpha^2<0$		
	v^1, v^2		$\pi(-\alpha^2)$	
$^1S_0$, $^3S_1$	[see (i)]		$\pi_0^{ii}=-\pi/4\lambda a_i(a_i+\alpha)^2$	(A1′)
			$\pi_0^{12}=-\pi/2\lambda(a_1+a_2)(a_1+\alpha)(a_2+\alpha)$	(A2′)
$^3D_1$	[see (i)]		$\pi_2^{ii}=-\pi(a_i^2+4a_i\alpha+5\alpha^2)/32\lambda a_i(a_i+\alpha)^4$	(A3′)
			$\pi_2^{12}=-[\pi/4\lambda(a_1+a_2)^3(a_1+\alpha)^2(a_2+\alpha)^2]\times[a_1^2a_2^2+2a_1a_2(a_1+a_2)\alpha+(a_1^2+3a_1a_2+a_2^2)\alpha^2]$	(A4′)
$^1P_1$, $^3P_{0,1,2}$	[see (i)]		$\pi_1^{11}=-\pi(a+3\alpha)/16\lambda a(a+\alpha)^3$	(A5′)
			$\pi_1^{12}=$ Eq. (A3′)	
			$\pi_1^{22}=-[\pi/256\lambda a(a+\alpha)^5]\times(5a^3+25a^2\alpha+47a\alpha^2+35\alpha^3)$	(A6′)
$^1D_2$, $^3D_{2,3}$	[see (i)]		$\pi_2^{11}=$ Eq. (A3′)	
			$\pi_2^{12}=$ Eq. (A6′)	
			$\pi_2^{22}=-[\pi/512\lambda a(a+\alpha)^6]\times(7a^4+42a^3\alpha+82a^2\alpha^2+122\alpha^3a+63\alpha^4)$	(A7′)

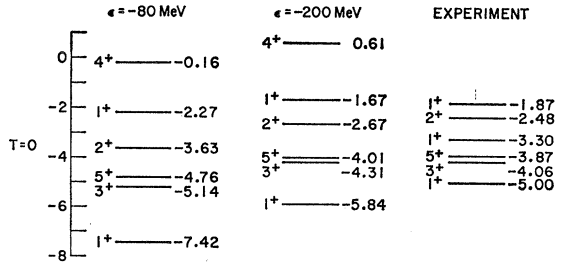

FIG. 16. The $T=0$ spectra for the $A=18$ nucleus, obtained from diagonalizing $K(\epsilon)$ for $\epsilon=-80$, -200 MeV in an oscillator basis. The experimental spectrum is displayed for comparison.

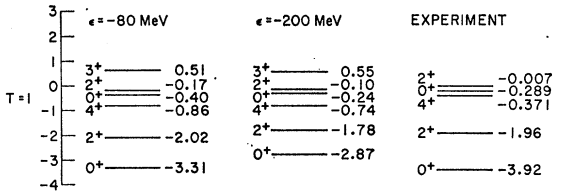

FIG. 17. The $T=1$ spectra for the $A=18$ nucleus obtained from diagonalizing $K(\epsilon)$ for $\epsilon=-80$, -200 MeV.

separable potential (b) can provide a reasonably accurate reproduction of the standard local potentials.

One might wish to question the significance of these latter statements on the grounds that the free two-nucleon potential is unlikely to be separable. We can defend our calculations on two fronts. First, there is the conventional statement that the free-space interaction is definitely known to be local only for large nucleon-nucleon separations. At small internucleon distances it is hard to justify the existence of a potential, let alone to establish its locality. Second, our residual interaction and the one derived in comparable situations from the HJ potential are not radically different. Indeed, the differences which are obtained in the nuclear matrix elements are perhaps an indication of the latitude one can expect in the ultimate calculation of spectra. One may view as extreme determinations from our potentials, the interaction obtained from an oscillator spectrum with no gap [Table V, column (a)] and the interaction arising from the propagator $Q(E'-T)^{-1}Q$ [Table IX, column (a)]. An adequate representation of these extremes is obtained from the $K(\epsilon)$ spectra for $\epsilon=-80$ MeV and $\epsilon=-200$ MeV. In Figs. 16 and 17, we present the $A=18, T=0$ and $T=1$ spectra obtained in these two situations. A more reasonable fit to the experimental level positions results for the choice $\epsilon=-200$ MeV and corresponds to plane-wave intermediate states. Such a fit must be viewed as premature and fortuitous, since we have not included core-polarization forces. In addition, the present authors intend to show that the use of more realistic Wood-Saxon wave functions has an appreciable effect on the calculated $A=18$ spectra.

Note added in proof. The authors would like to thank D. M. Clement and I. R. Afnan for having pointed out an error in our calculation of the D-state probability.

APPENDIX

We list in Table XI the various functions

$$\pi_l^{ii'}=P\int_0^\infty q^2dq\, v_l^i(q)v_l^{i'}(q)[\epsilon-(\hbar^2/m)q^2]^{-1}$$

discussed previously. We introduce the notation $\lambda=\hbar^2/m$, $\epsilon_i=\lambda a_i^2$. We have given $\pi_l^{ii'}(\epsilon)$ for $\epsilon>0$ and $\epsilon<0$, spearately. For the latter case we also introduce $\epsilon=-\lambda\alpha^2$.